

UCSF

UC San Francisco Electronic Theses and Dissertations

Title

Increased intracellular pH is necessary for epithelial and embryonic stem cell differentiation

Permalink

<https://escholarship.org/uc/item/3r3303px>

Author

Ulmschneider, Bryne

Publication Date

2016

Peer reviewed|Thesis/dissertation

Increased intracellular pH is necessary for epithelial and embryonic
stem cell differentiation

by

Bryne Ulmschneider

DISSERTATION

Submitted in partial satisfaction of the requirements for the degree of

DOCTOR OF PHILOSOPHY

in

Biochemistry and Molecular Biology

in the

GRADUATE DIVISION

of the

UNIVERSITY OF CALIFORNIA, SAN FRANCISCO

Dedication

My thesis is dedicated to my family, biological and chosen, whose unwavering belief in me kept me going when I wanted to stop believing in myself. In particular, this thesis is dedicated to my father. My journey through graduate school has been a personal journey as well as a scientific one, and my father's lasting presence in my life despite his death early in my graduate career has changed entirety of my graduate school experience. I know that he would have been deeply proud of me for the completion of my PhD.

Acknowledgements

Many people contributed to the success of this project. Firstly, I'd like to thank my labmates for their help and contributions. In particular, I thank Sumitra Tatapudy for assistance with image acquisition of mCherry::pHluorin for pH measurements involving CG8177, Marimar Benitez for screening through candidate solute carrier genes genes, and my former colleague Dinara Azimova for help with the initial experiments identifying the Hedgehog pathway as an important component of the pHi signaling network.

Secondly, I'd like to thank several members of the Barber laboratory for their instrumental help in this project. I'd like to acknowledge the enormous contribution of Bree Grillo-Hill and Diane Barber who conducted the mESC experiments described in this work. In particular, Diane Barber measured intracellular pHi, Bree Grillo-Hill cultured cells and performed FACS analysis and embryoid body assays. I performed RNA extraction, and qPCR of mESC cells for the gene expression data, and analyzed and compiled results and graphs in collaboration with Bree Grillo-Hill. I also thank Bree Grillo-Hill for continuous advice and support during the completion of this work, particularly in helping me design the methodology for quantitative imaging.

I'd also like to thank Bradley Webb for assistance with quantitative pHi imaging analysis

and Torsten Wittmann and members of the Wittmann, Barber, and Nystul labs for helpful discussions. I'd also like to thank my thesis committee members Diane Barber and Tom Kornberg for their advice and direction in the completion of this project.

My funding was supported by a fellowship from the California Institute of Regenerative Medicine, TG2-01153. Additional funding for this work was also supported by National Institute of Health grants GM097158 to TGN, GM47413 to DLB, and GM116384 to DLB and TGN.

Abstract

I found that an increase in intracellular pH is required for the differentiation of both a *Drosophila* epithelial stem cell lineage and mouse embryonic stem cells. This is the first demonstration of a role for intracellular pH in the regulation of stem cell differentiation, and our discovery of its importance in two different types of stem cell lineages suggests that this function for intracellular pH may be broadly conserved. In the *Drosophila* epithelial stem cell lineage, my findings support a model in which increased intracellular pH promotes terminal differentiation to a “stalk cell” fate by attenuating Hedgehog signaling, possibly through post transcriptionally regulating Smoothed levels. Our study of embryonic stem cells reveal that increased intracellular pH is required for differentiation measured by a battery of several different assays. Collectively, these findings demonstrate that intracellular pH can fine tune the process of cell differentiation, which opens up a new direction for understanding how cell physiology can influence cellular signaling.

Contents

Overview and Scope	
Physiological changes and stem cells	1
Intracellular pH and cell biology.....	2
Hedgehog signaling	4
<i>Drosophila</i> follicle stem cell biology.....	5
Wnt pathway.....	6
Hedgehog pathway	6
Specification of follicle cell types	6
mESC background	8
Results	
Intracellular pH is increased in FSC.....	10
Intracellular pH is required for proper FSC differentiation	13
Increased intracellular pH promotes excessive follicle cell differentiation...	18
Increased intracellular pH attenuates Hh signaling.....	20
Conclusions	
Conclusions and speculations from <i>Drosophila</i> Data.....	22
On pHi measurements and variability.....	26
mESC results	29
Methods:	
pHluorin quantitative imaging	35
<i>Drosophila</i> tissue immunofluorescence staining	38
Quantitative Microscopy: Ptc-pelican-GFP <i>quantitative analysis</i>	38

Egg laying assays.....	39
Quantitative Microscopy for Smo::GFP quantitative analysis.....	39
Plotting and Statistics	39
Stocks	40
Mouse Embryonic Stem Cell Culture	41
qRT-PCR experiments	42
References	43
Appendices	
Code Appendix.....	52

List of Figures

Figure 1: Hh signaling overview	7
Figure 2: The follicle stem cell lineage	9
Figure 3: Calibrating pHlouring in follicle cell tissue	12
Figure 4: Intracellular pH changes during differentiation and in reponse to <i>DNhe2</i> knockdown	14
Figure 5: <i>DNhe2</i> is necessary for proper oocyte formation and fertility	16
Figure 6: <i>DNhe2</i> is necessary in the FC lineage for proper cell specification	17
Figure 7: pHi increases correlate with stalk differentiation defects	19
Figure 8: Notch pathway activity is not affected by pHi.....	23
Figure 9: Hh pathway activity decreases when pHi increases	23
Figure 10: Increased pHi rescues moderately upregulated Hh activity	25
Figure 11: Increased pHi decreases Smoothened levels	27
Figure 12: Model for effects of Hh and pHi on stalk formation.....	27
Figure 13: Increased pHi is necessary for mESC differentiation.....	33
Figure 14: mESC differentiation effects are specific to Nhe2	36

List of Tables

Table 1: Comparison of three and two point calibrations	30
Table 2: All pHi experiments, comparison of controls	30

Overview and Scope

Physiological changes and stem cells

Regenerative medicine's great promise holds that we will someday have the ability to direct cell differentiation to grow complete, fully functional organs *in vitro*. However, this promise remains mostly unfulfilled as the furthest advances in tissue regeneration *in vitro* can currently only approximate the organs they are meant to duplicate. Although we have made substantial progress in directing differentiation of specialized cell types that approximate their *in vivo* correlates for brains (Lancaster et al. 2013), lungs (Dye et al. 2015), and insulin producing cells, amongst others, these cells often lack important features of their *in vivo* counterparts (Pagliuca and Melton 2013; Robinton and Daley 2012). This indicates that at a fundamental level, our understanding of important features of differentiation is still incomplete. Further investigation into additional levers that control the developmental process are required before we can truly fulfill the promise of regenerative medicine.

More specifically, far less is known about physiological changes that occur during the process of differentiation than large scale transcriptional and epigenetic changes. We understand that stem cells need to coordinate the activity of multiple cellular pathways and much of the stem cell field has focused for many years on elucidating those pathways and the genetic mechanisms by which they are controlled. Along those lines, in addition to classic developmental pathways, scientists are starting to explore other cytosolic factors involved in differentiation and how they impact differentiation. Several recent papers have examined redox and calcium signaling as components of stem cell differentiation.

First, in mouse neural stem cells (Khacho et al. 2016) demonstrated that impairment of mitochondrial structure via manipulation of mitochondrial fission and fusion machinery impaired neural stem cells' ability to self-renew due to increased levels of reactive oxidative

species (ROS) and that differentiated cells have higher levels of ROS. In *Drosophila* another paper looked at how Wnt2 and Wnt4 regulate antioxidant genes to maintain low levels of ROS signaling in the germline stem cell (GSC) niche and further showed that low levels of ROS are necessary for GSC differentiation (Wang et al. 2015). Finally, In the *Drosophila* haematopoietic cell lineage, moderately high levels of ROS moderately high levels of ROS primes cells for differentiation (Owusu-Ansah and Banerjee 2009). These papers show that redox state, a cytosolic factor, is an important component of maintaining the stem cell's ability to self-renew and differentiate.

Additionally, *Drosophila* intestinal stem cells were shown to use calcium signaling to regulate proliferation after activation by the metabolite L-glutamate (Deng, Gerencser, and Jasper 2015). This body of work suggests cytosolic factors act both upstream and downstream of signaling pathways respond and integrate environmental signals.

My thesis work is the first to uncover intracellular pH as an additional cytosolic factor that fine tunes the differentiation process of epithelial and embryonic stem cells. I show that *DNhe2*, the *Drosophila* ortholog of mouse *Nhe1* is required for the proper formation of the follicle epithelium, and segregation of cell fates within the follicle epithelium and cause corresponding changes in pHi. Furthermore, we show that inhibiting pHi changes in mESCs blocks differentiation. Finally, I show that pHi changes can attenuate Hedgehog signaling. Taken together this suggests that changes in pHi help promote differentiation across different tissues and organisms.

Intracellular pH and cell biology

pHi changes are important in regulating diverse cellular processes such as cell migration, cancer metastasis, aging and the regulation metabolic pathways. Changes in pH are necessary for directed cell migration (Denker and Barber 2002; Martin et al. 2011) and increasing cytosolic pH is sufficient to drive cancer progression (Grillo-Hill Bree K Choi Changoon; Jimenez-Vidal Maite Barber 2015). Changes in pHi detect metabolic changes

during growth in yeast (Isom et al. 2013; Dechant et al. 2010). pHi regulates lifespan in yeast through the vacuolar proton pump VMA1 (Hughes and Gottschling 2012). This acidification of the vacuole is regulated by plasma membrane proton ATPase (PMA1) which is divided asymmetrically between mothers and daughters (Henderson, Hughes, and Gottschling 2014).

How pHi regulates cellular processes can vary. I believe changes in cytosolic pH is a method for cell signaling, either directly or as a post-translational modification, similar to phosphorylation or ubiquitination, a view which is gaining growing acceptance in the cell biology field (Schönichen et al. 2013; Orij, Brul, and Smits 2011).

The evidence for protons as a direct signaling molecule comes from work in *C. elegans* demonstrating that pHi oscillations are both necessary and sufficient for inducing muscle contractions. Firstly, a sodium-proton exchanger, *pbo-1*, acidifies the intracellular space between intestine and muscle acidification is both necessary and sufficient to cause muscle contractions (Beg et al. 2008). The sufficiency of caged protons to induce muscle contractions demonstrates that protons act directly as a signaling molecule. Next, sodium-proton exchange is an important signaling event in intestinal cells. Calcium oscillations in the intestine acts upstream of pHi (Wagner et al. 2011), and pHi oscillations in both the muscle cells via NHX-7 and intestinal cells via NHX-2 are required for correct timing and of muscle contractions (Pfeiffer, Johnson, and Nehrke 2008).

Evidence for protons as a second messenger come from a number of studies showing that protein residues with a pK_a within the range of 7.0 - 7.4 can affect phosphorylation events and binding affinity. These pH-sensitive proteins are referred to as pH sensors. One example of a pH sensor is focal adhesion kinase (FAK) which is sensitive to changes in pH at a histidine residue which affects phosphorylation events necessary for FAK activation (C. H. Choi et al. 2013). Another pH sensor is G(α), a G-protein coupled receptor.

G(α) is phosphorylated in response to changes in cellular pH induced by glucose starvation or acetic acid treatment (Isom et al. 2013). A pH sensor that affects specificity of binding are guanine nucleotide exchange factors (GEFs) binding to phosphoinositides (Frantz et al. 2007). This paper demonstrated that, again, a histidine residue with a pK_a within the physiological range was pH sensitive, and that pH sensitivity affected the binding specificity of a GEF catalyzing the GTP-exchange during cell migration events. Altogether this evidence shows pHi is involved in regulating signaling in many different cellular contexts to help coordinate and regulate signaling cascades.

Hedgehog signaling

Hedgehog signaling is a critical developmental pathway implicated in embryonic development, differentiation and some types of cancer. In the absence of Hedgehog ligand, the hedgehog receptor, *patched* (*ptc*) inhibits *smoothened* (*smo*), which remains in intracellular vesicles, and is ubiquitinated and then degraded (S. Li et al. 2012). Upon ligand binding, inhibition of *smo* is relieved by a mechanism that involves a change in conformation in the C-terminal tail of *Smo* (Chen et al. 2010) and phosphorylation of residues in the C-terminal tail by CK1 and PKA (Zhao, Tong, and Jiang 2007; C. Zhang et al. 2004). After *Smo* phosphorylation, a complex involving Costal2 (*Cos2*), SuFu (suppressor of Fused) and Fu is derepressed resulting a switch from the inactive to active state of the transcription factor *ci* in flies (see Fig. 1 for summary) or Gli in mammals.

One current model of the mechanism by which *ci* switches to its active conformation is that phosphorylation of *Smo* is required for *Ci* to switch from the repressed to active form (Apionishev et al. 2005). Interestingly, the same kinases required for *Smo* activation, CK1 and PKA, also phosphorylate *Ci* to target it for proteolytic cleavage to *Ci^R* (Price and Kalderon 2002; Smelkinson, Zhou, and Kalderon 2007; Jia et al. 2005). One current model explaining the mechanism of *Ci* activation in response to Hh ligand is that increases in Hh ligand lead to progressive increases in *Smo* phosphorylation which lead to dimerization

of the Fu-Cos2 complex at the Smo C-terminal tail which regulates the SuFu-Ci complex, leading to conversion to activated Ci (Shi et al. 2011).

***Drosophila* follicle stem cell biology**

Drosophila ovaries are composed of multiple ovarioles, and two follicle stem cells (FSCs) reside within niches at the anterior tip of each ovariole in a structure called the germarium (Margolis and Spradling 1995; Nystul and Spradling 2007). The FSCs divide regularly during adulthood to self-renew and produce daughter cells that differentiate into the functional cells of the follicle epithelium. Newly produced FSC daughter cells, called prefollicle cells, are found just downstream from the FSC niche in Region 2b of the germarium (Fig. 2A).

Immediately upon exiting the niche, a subset of prefollicle cells begin to differentiate into polar and stalk cells (Tworoger et al. 1999; Larkin et al. 1996a; Besse, Busson, and Pret 2002; Nystul and Spradling 2010), which are specialized cell types that reside at the poles and in between follicles, respectively, while the remaining prefollicle cells differentiate into main body follicle cells that surround the developing germline cyst. The main body follicle cell lineage is marked by *eya*, which must be downregulated to allow proper stalk formation and the expression of *castor* (Chang et al. 2013b). This well-defined lineage makes it possible to identify the stem cell and distinct stages of differentiation *in vivo* with single-cell resolution.

Several common signaling pathways are involved follicle stem cell lineage decisions. The EGFR and Wnt pathway are primarily involved in maintaining stem cell identity. Hedgehog pathway seems to be involved in both stem cell maintenance and differentiation decisions. The Notch and JAK-STAT pathways play important roles in specifying stalk and polar cell fates. The places where these pathways are active in the follicle cell lineage is summarized in Fig 2b.

Wnt pathway

The Wnt pathway (*wingless* in *Drosophila*) is important for both stem cell maintenance and differentiation. The *wingless* ligand comes from both cap and terminal filament cells, as well as escort cells (Sahai-Hernandez and Nystul 2013). Both positive regulators of the pathway, *dishevelled* (*dsh*) and *armadillo* (*arm*) as well as negative regulators *shaggy* (*sgg*) and *axin* cause stem cell loss (Song and Xie 2003). This suggests that wnt signaling is tightly regulated around a narrow range. Additionally, overactive wnt signaling resulting from loss negative regulators can impact proper differentiation and organization of the epithelium. Stalk cells, which are normally quiescent, remain mitotically active, and late stage egg chambers have disorganized epithelia.

Hedgehog pathway

Hedgehog signaling plays a role in stem cell maintenance, proliferation and cell fate determination. FSCs lacking *smo* are rapidly lost from the FSC niche, indicating *smo* is necessary for differentiation (Kirilly et al. 2005). Hedgehog is also sufficient for inducing proliferation in stalk cells, indicating that in normal differentiation downregulation of hedgehog likely controls when stalk cell precursors stop dividing (Besse, Busson, and Pret 2002; Y. Zhang and Kalderon 2000; Tworoger et al. 1999; Forbes, Lin, et al. 1996; Forbes, Spradling, et al. 1996); (Besse, Busson, and Pret 2002; Y. Zhang and Kalderon 2000; Tworoger et al. 1999; Forbes, Lin, et al. 1996; Forbes, Spradling, et al. 1996)). Hedgehog is likely involved earlier than notch in determining cell fate to first specify cells as pre-stalk or polar (Tworoger et al. 1999; Besse, Busson, and Pret 2002; Chang et al. 2013b; Yan Zhang and Kalderon 2001). Loss of PKA is sufficient to rescue normal proliferation patterns (Yan Zhang and Kalderon 2001) whereas fused is required for differentiation of stalk cells, but not proliferation (Besse, Busson, and Pret 2002).

Specification of follicle cell types

Figure 1: Hh signaling overview

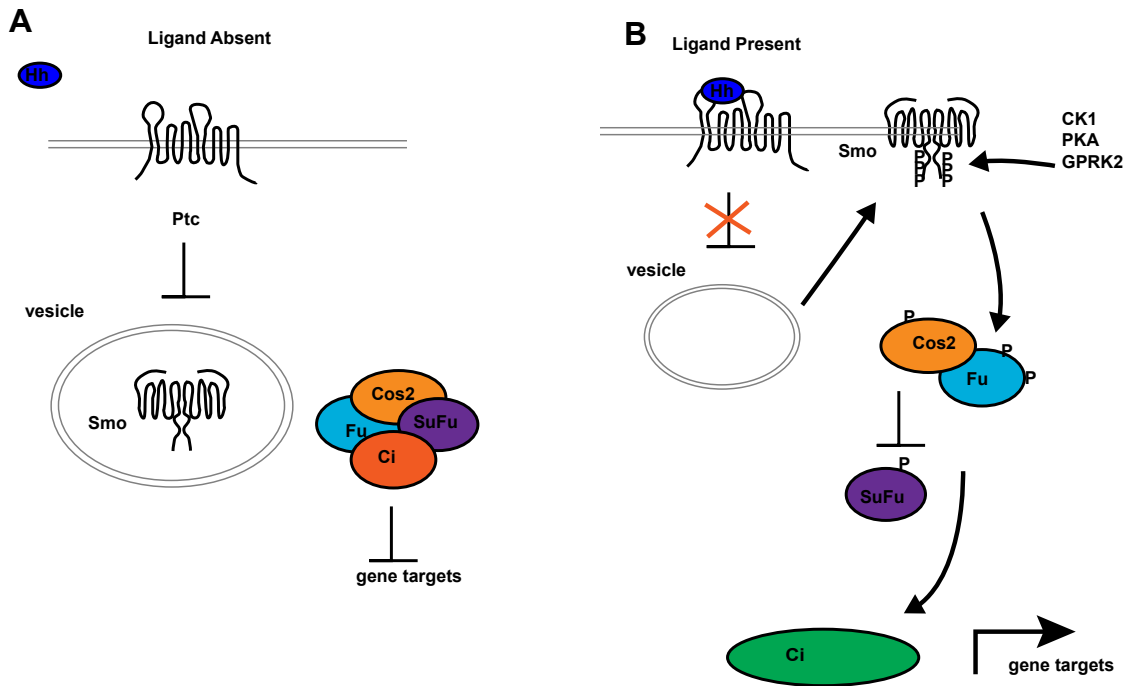


Figure 1: a) in the absence of Hh ligand, ptc, a 12-pass transmembrane protein negatively regulates smoothed (smo), which remains in intracellular vesicles, away from the cell membrane. A complex involving Fused, Suppressor of Fused and Cos2 keeps Ci, the Drosophila homologue of Gli, in its repressive, uncleaved form. b) When Hh binds to ptc, repression of smo is relieved, smo translocates to the membrane and residues at the C-terminal are phosphorylated by CK1, PKA and GPRK2. Smo phosphorylation then triggers phosphorylation of Cos2 and Fused, which represses SuFu. This triggers proteolytic cleavage of Ci into its active form, which then leads to transcription of Hh pathway targets.

The current model for the specification of stalk and polar cell fate involves both Notch and JAK-STAT signaling. It was first observed that Notch pathway is both necessary for stalk formation and sufficient to induce polarity defects(Larkin et al. 1996b). Later work demonstrated through lineage tracing that both stalk and polar cells arise from a Hh-dependent precursor population(Tworoger et al. 1999). The current model is that high levels of Notch signaling receiving the Notch ligand Delta from the germline induce a small portion of prestalk/prepolar cells to become polar cells. Polar cells then produce the JAK-STAT ligand Unpaired, which activates the JAK-STAT pathway only in the stalk cells (Assa-Kunik et al. 2007)).

Two additional genes, *castor (cas)* and *eyes absent (eya)* are also involved in the specification of follicle cell types. *Eya* is expressed in main body, but neither stalk nor polar cells, and is a Notch-dependent (Adam and Montell 2004) necessary repressor of polar and stalk cell fate(Bai and Montell 2002; Chang et al. 2013b). *Castor* is required to for stalk cell formation, and partially required for stem cell maintenance (Tworoger et al. 1999; Besse, Busson, and Pret 2002; Chang et al. 2013b; Yan Zhang and Kalderon 2001). *Castor* and *Eya* are initially expressed together early in follicle cell differentiation, where Hh activity is high. Hh acts to repress *Eya* to allow *castor* to turn on, and then subsequently for polar and then stalk cell specification. *Castor* is upstream of the Notch and JAK-STAT pathways, because it remains on in both polar and stalk cells (Tworoger et al. 1999; Besse, Busson, and Pret 2002; Chang et al. 2013b; Yan Zhang and Kalderon 2001).

mESC background

mESCs are thought to mimic the earliest stages of embryonic development (Murry and Keller 2008a). mESC lines serve as a model system for probing the earliest decisions in embryonic development. Three different types of pluripotent mESC cells are commonly used. Stable mESC lines are derived from the inner cell mass of a developing embryo

Figure 2: The follicle stem cell lineage

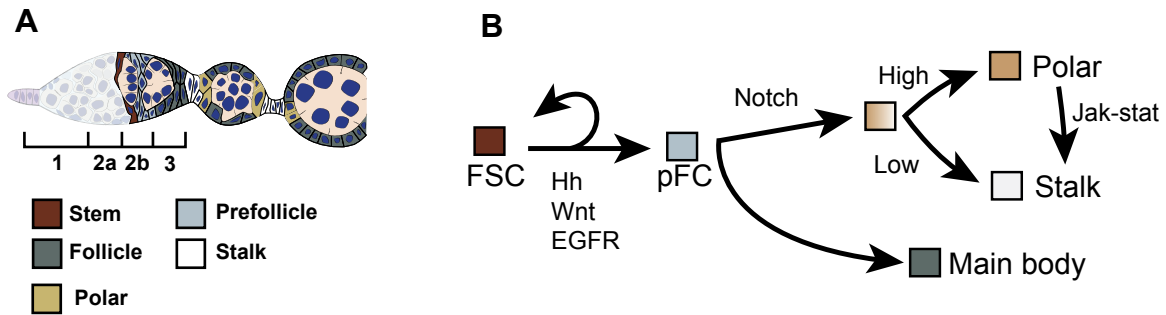


Figure 2: a) Structure of the germarium with the four regions, Region 1, 2a, 2b, and 3, indicated. Two FSCs (brown) are located in the middle of the germarium, at the Region 2a/2b border. Cells that exit the FSC niche become prefollicle cells (light grey) and then differentiate into main body follicle cells (dark grey), polar cells (tan), or stalk cells (white). Nuclei are shown in blue. b) A general schematic for important determinants in the follicle stem cell lineage. EGFR and Wnt are important for follicle stem cell (FSC) maintenance. Hh must be downregulated in order for prefollicle cells to make a lineage commitment. Further downstream, Notch ligand from the germline helps determine polar and stalk cell specificity. High levels of notch will lead to cells adopting a polar fate, which then produce Jak-Stat ligand to commit and maintain stalk cells.

and are classically defined as cells that are capable of forming mesoderm, ectoderm, and endoderm; can form all cell types injected into an organism as a teratoma, and capable of developing into a complete embryo after implanted. Naive mESCs are maintained in the presence either LIF (leukemia inhibitory factor) and serum or LIF and a cocktail of inhibitors for GSK3 and MEK (2i). LIF alone is insufficient to maintain naïve mESCs in a serum free media (Q. L. Ying et al. 2003). The addition of cocktail of inhibitors for GSK3 β and MEK form a more homogenous culture, and eliminate the requirement for serum, (Wray, Kalkan, and Smith 2010; Q.-L. Ying et al. 2008).

A final type of pluripotent cells are epiblast cells. The first step of differentiation either *in vitro* or *in vivo* is the formation of an epiblast post-implantation. Epiblasts differ from naive mESCs in that while they can form embryoid bodies and the three germ layers *in vitro*, they do not form chimaeras or complete embryos, and in fact can delay the development of a post-implantation embryo (Tesar et al. 2007). The genomic profile, and chromatin state of Epiblast cells are thought to be more similar to hESC, and distinct from naive mESCs. Studying the differences between epiblast and naive mESCs can give insight into the developmental changes between a pre and post-implantation embryo before any distinct lineage commitment.

Results

Intracellular pH is increased in FSC

Given emerging evidence that intracellular pH (pHi) dynamics regulates diverse cell behaviors (Schönichen et al. 2013), I asked whether changes in pHi may be part of normal cellular differentiation programs. I measured pHi of cells in the follicle epithelium using the FLP-out system (Pignoni and Zipursky 1997) to generate FSC clones expressing a genetically encoded pH biosensor pHluorin fused to mCherry (C.-H. Choi et al. 2013; Grillo-Hill et al. 2015; Koivusalo et al. 2010; Rossano, Chouhan, and Macleod 2013).

The fluorescence of mCherry is insensitive to physiological changes in pHi and indicates biosensor abundance, whereas the fluorescence intensity of pHluorin is an index of pHi within the physiological range (Miesenböck, De Angelis, and Rothman 1998), with increased intensity at higher pHi.

To determine how robustly pHluorin::mCherry worked in *Drosophila* ovarian tissue, I first had to calibrate pHluorin to mCherry fluorescence ratios to pH values. We would expect pHluorin to mCherry ratios increase linearly with pHi in follicle tissues that have equilibrated with a pH of a set value. Examples of follicle cell tissue equilibrated with a buffer of pH = 6.5 (Fig. 3A) has a much lower ratio value than tissue equilibrated with a buffer of pH = 7.5 (Fig. 3B). I used Concanavalin A conjugated to a 633 fluorophore to outline cell membranes in order to achieve single cell resolution (Fig. 3A',3B').

Using Concanavalin A as a reference for cell to cell boundaries, I then identified distinct populations stem, prefollicle and follicle cells, identified by their location in the germlaria, with the stem cell as the anterior-most cell in a clone generated with actin-FLPout-gal4, prefollicle as cells within region 2b, and follicle cells as cells in region 3.

I drew a background region of interest (ROI), and then subtracted the average intensity from the background ROI from each z-slice in order to remove interference from background intensity. I customized a plugin adapted from an ImageJ plugin called "BG Subtraction from ROI."

After quantifying the ratio on background subtracted images in ImageJ, I found that ratios did increase linearly with increasing pH (Fig. 3C), and every cell type had robust r^2 values of 0.85 or greater (see table 1, three point calibration, and Fig. 3C). I also confirmed that a two-point calibration curve is virtually unchanged from a three-point calibration curve (compare Fig. 3C to 3D, and Table 1, differences), and proceeded to use a two-point

Figure 3: Calibrating pHluorin in follicle cell tissue

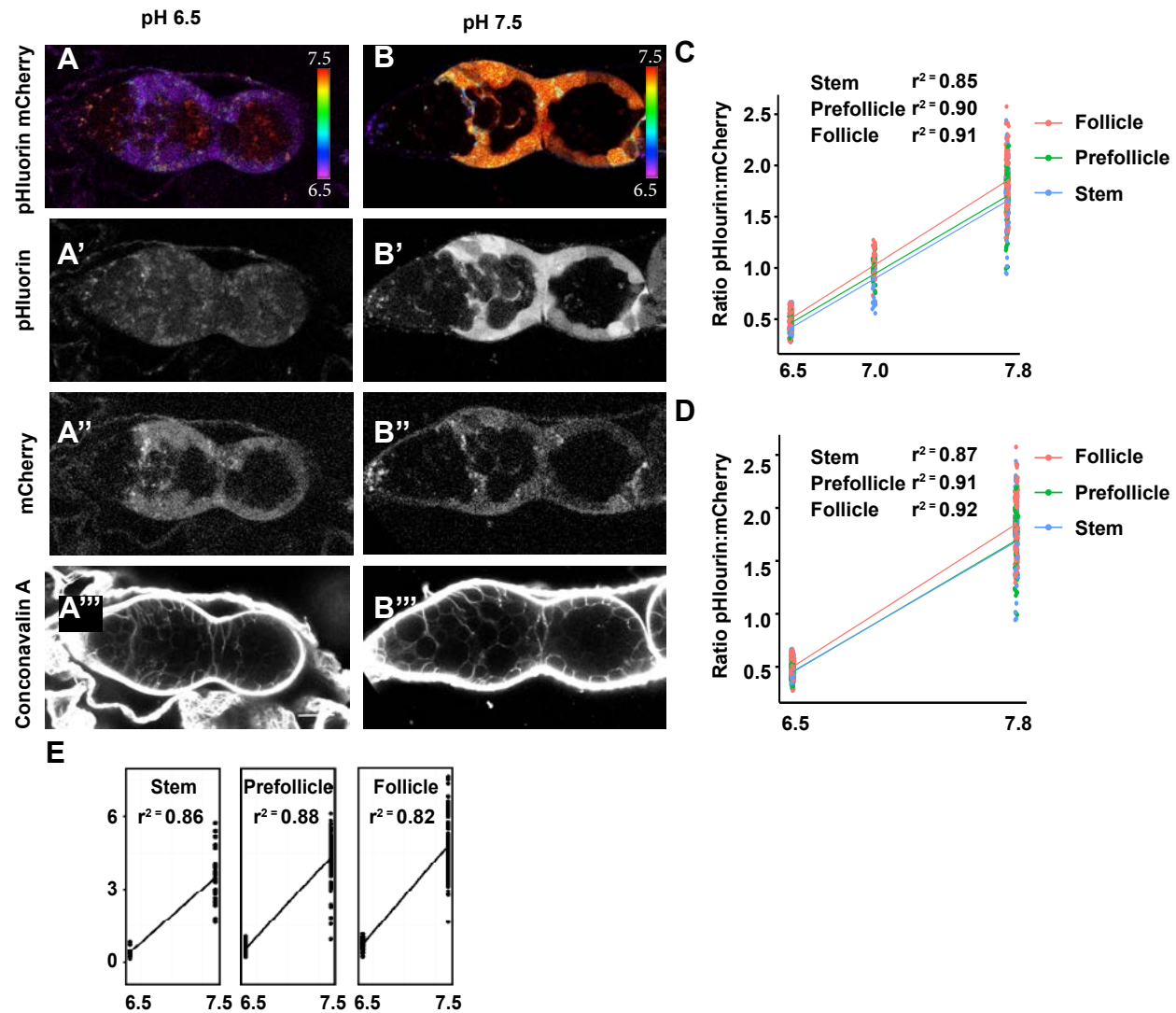


Figure 3: a-b) Germaria in nigericin buffer with pHi equilibrated to pH = 6.5 (a) or 7.5 (b). In these conditions, the ratio of pHluorin fluorescence to mCherry fluorescence became uniform throughout the germaria, with low pHluorin fluorescence intensity at a pH of 6.5 and high pHluorin fluorescence intensity at a pH of 7.5. The pseudocoloring indicates the ratio of the fluorescence intensities of pHluorin to mCherry, which correlates with pHi. Scale bar indicates pHi. For pHi measurements, germaria were stained with Concanavalin A conjugated to Alexa-Fluor 647 (a'''-b''') to identify cell boundaries to ensure each cell could be accurately measured independently. c) Three point measurement for FSCs, prefollicle cells, and follicle cells of FSC clones expressing mCherry::pHluorin in freshly dissected ovarioles equilibrated ovarioles to a pH of 6.5, 7.0, or 7.8 in buffers containing the protonophore nigericin. The average ratio of pHluorin to mCherry fluorescence increased linearly with increasing pH for each cell type ($r^2 = 0.85$ for stem, 0.90 for prefollicle, and 0.91 for follicle cell types), confirming that the biosensor is responsive to pH changes as predicted when expressed in the follicle epithelium. d) Representative calibration curves for a typical experiment, in this case wildtype FSC clones with mCherry::pHluorin. r^2 values are indicated on graph.

calibration for subsequent experiments. An example of a typical two-point calibration, which I did for every replicate of every experiment, has r^2 values greater than 0.70 (Fig. 3E).

Using this calibration method, I determined the pHluorin to mCherry fluorescence ratios in FSCs, prefollicle cells, and follicle cells of ovarioles dissected in a bicarbonate buffer, which preserves tissue health and activity of bicarbonate transporters, and then used identical image acquisition settings to generate a two-point calibration curve for each cell type from samples incubated in nigericin buffers (Fig. 4A-B). I found significant differences in pHi for each cell type, with higher values at progressively later stages of differentiation (6.8 ± 0.07 for the FSCs, 7.0 ± 0.06 for the prefollicle cells, and 7.3 ± 0.05 for the follicle cells; $p < 0.001$; $n = 36$ germaria). To determine the role of increased pHi in follicle cell differentiation, I next looked at *DNhe2*, which was previously reported as the likely ortholog of the mammalian ubiquitously expressed plasma membrane Na-H exchanger NHE1 (Grillo-Hill et al. 2015) that catalyzes the electroneutral influx of extracellular Na^+ and efflux of intracellular H^+ . I knocked down *DNhe2* expression via RNAi with a follicle cell specific driver (FC-gal4), and found that pHi decreases by a statistically significant amount of about 0.2 pHi units in prefollicle and follicle cells (Fig. 4C)

Intracellular pH is required for proper FSC differentiation

To determine the role of increased pHi in follicle cell differentiation, I investigated the phenotype caused by loss of *DNhe2*. I first observed that flies homozygous for *DNhe2^{null}*, a null allele that lacks the entire *DNhe2* open reading frame, that are viable (Grillo-Hill et al. 2015), but have substantially reduced fertility and fitness. The *DNhe2^{null}* flies lack robust health, grow more slowly and are weakly fertile. They lay, on average, about half the number of eggs wildtype flies lay (Fig. 5A). Noting that there is a defect in oogenesis, I examined the structure of the ovariole by staining with FasIII to look at follicle cells and Vasa to look at germline and found that 45% of *DNhe2^{null}* ovarioles exhibited distinct

Figure 4: Intracellular pH changes during differentiation and in response to *DNhe2* knockdown

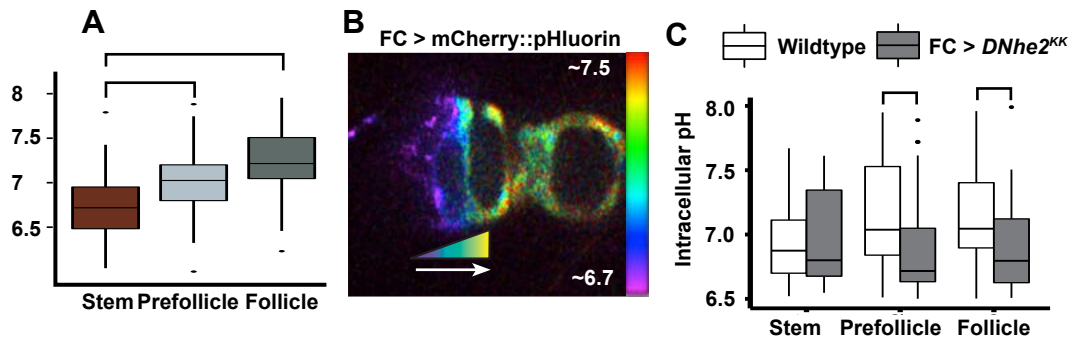


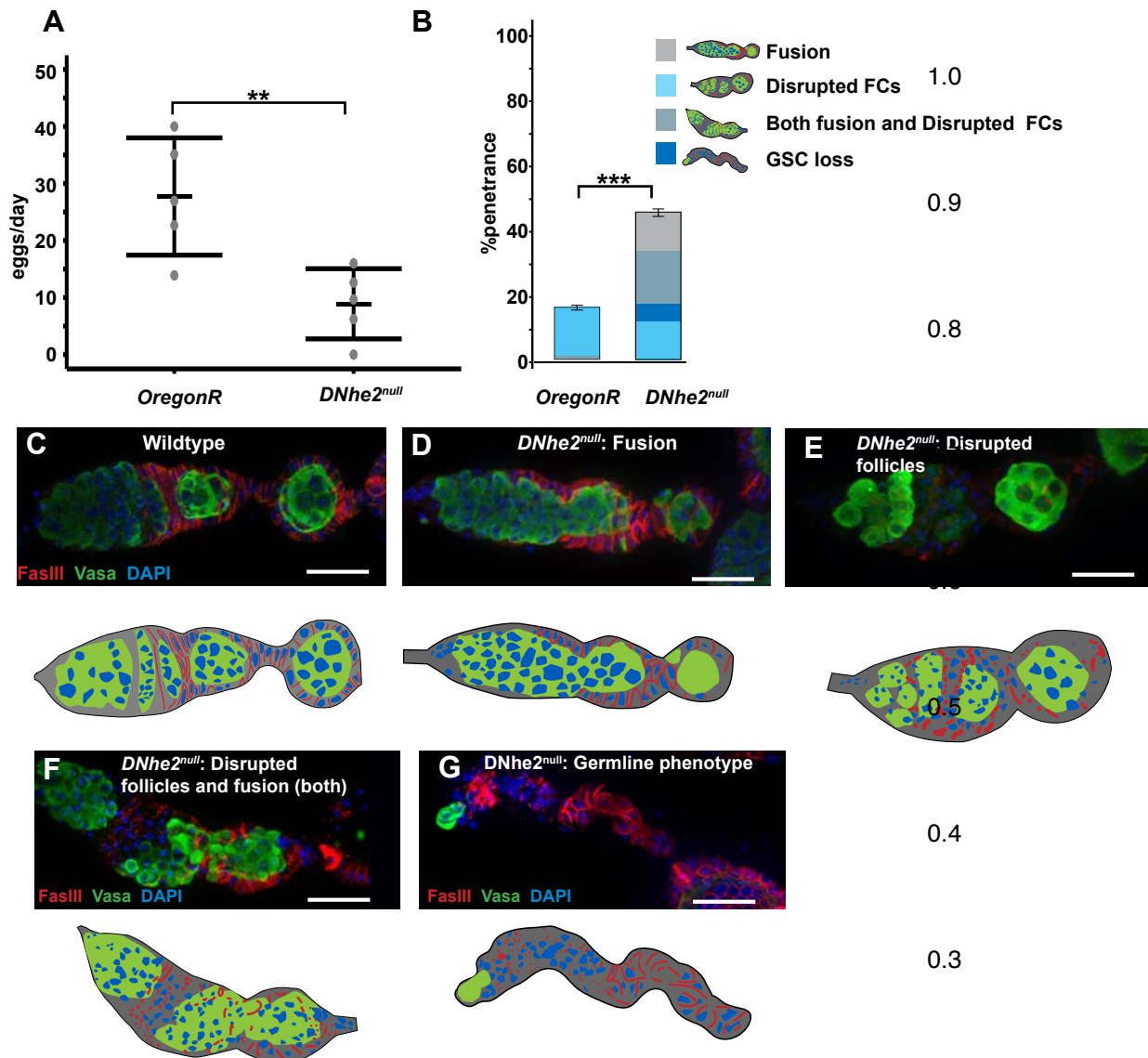
Figure 4: a) Intracellular pH increase as cells transition from an FSC to a follicle cell within the gerarium (n = 36 germaria; N = 5 independent replicates). b) A gerarium expressing UAS-mCherry::pHluorin in an FSC clone generated with the FLPout system. The pseudocoloring indicates the ratio of the fluorescence intensities of pHluorin to mCherry, which correlates with pHi. Scale bar indicates pHi. c) *Nhe2*^{KK} RNAi driven in follicle cells with FC-Gal4 (grey boxes) causes a significant decrease in pHi compared to control (white boxes) in prefollicle and follicle cells. (n = 16-17 germaria; N = 3 independent replicates)

morphological defects in the encapsulation and budding of follicles from the germarium.

These phenotypes ranged from relatively mild fused germline cysts (Fig. 5D) to severe phenotype which fall into multiple categories. Phenotypes shown in Fig 5C-G progress from the most mild, to the most severe. Fig. 5D shows disrupted follicles which consist of follicles aren't in proper shape or alignment in relation to germline cysts. In wildtype follicle cells line up in a even monolayer, and in *DNhe2^{null}* ovaries with disrupted follicle cells no distinct monolayer is present, and additionally the membrane visualized via FasIII staining is not cohesive and fragments in places. Disrupted FCs and fusions alone each comprise 11.8% of the phenotypes. Ovarioles with both disrupted follicle cells and fused cysts, which have a more severe defect, comprise 21% of ovarioles. This means that these two phenotypes correlate with each other about half the time. Finally, in some cases, a subcategory of ovarioles in which cysts are fused and FCs are disrupted, germline is also lost, probably through progressive decline of GSCs. The fact that these phenotypes tend to resolve later on in development, still forming more normal cysts later downstream and can produce fertile eggs led me to further characterize the phenotypes within the ovariole.

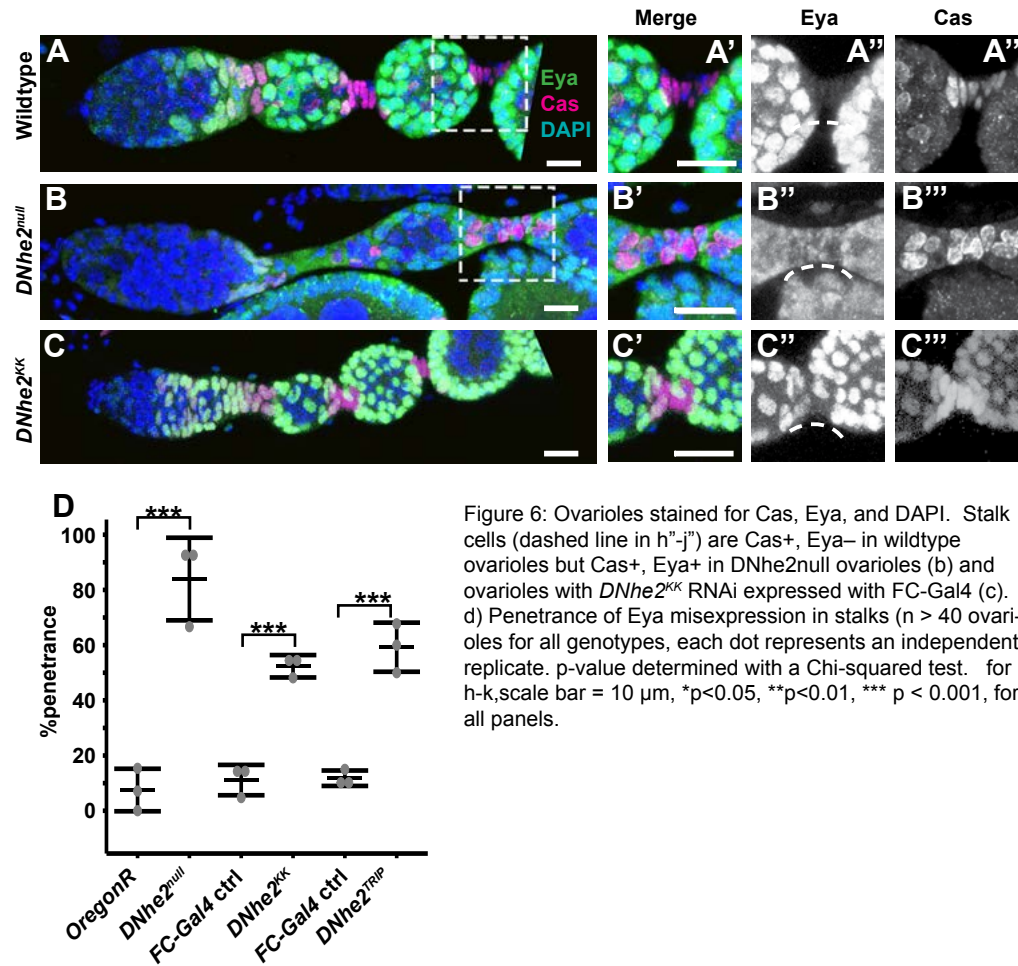
In wildtype tissue, prefollicle cells express both Castor (Cas) and Eyes absent (Eya), whereas stalk and polar cells are Cas⁺, Eya⁻ (Fig. 6A) (Chang et al. 2013a). In the *DNhe2^{null}* I found that cells in the first stalk downstream from the germarium remained Cas⁺, Eya⁺ (Fig. 6B) in 83% ± 9% (n = 42) of *DNhe2^{null}* ovarioles, compared with 9% ± 4% (n=86) of wildtype ovarioles (Fig. 6A). In addition, I found a similar phenotype upon RNAi knockdown of *DNhe2* specifically in follicle cells using two separate RNAi lines (Fig. 5C), though the penetrance was lower, suggesting that there are some non-cell autonomous effects on follicle cell differentiation in *DNhe2^{null}* flies or that knockdown with these RNAi lines is incomplete. I would predict that amongst *DNhe2^{null}* germaria without a distinct morphological defect that I measured, would have a Cas/Eya defect, but no morphological

Figure 5: *DNhe2* is necessary for proper oocyte formation and fertility



a) *DNhe2^{null}* flies lay fewer eggs per day than wildtype flies $n = 11-14$ flies in 5 independent replicates, pvalue is from Student's t-test. b) Quantification of various phenotypes found in *Dnhe2Null* flies. p-value is from a Fisher's Exact test; $n = 96$ (Wildtype) and $n = 136$ (*DNhe2null*) germaria; $N = 3 - 5$ independent replicates, error bars represent S.E.M. c) Wildtype germarium labeled with FasIII to label follicle cells, Vasa to label germline and DAPI. d-g) Examples of morphological phenotypes from *DNhe2^{null}* show d) follicle cells failed to properly encapsulate the germline resulting in fused cysts (labeled as Fusion in (b)), e) A lack of a follicle cell monolayer with fragmentation across the cell membrane. FasIII, when present is also localized more less laterally and more apical and basally and f)Both fused germline cysts and disrupted follicle cell morphology. This category represents 21% of germaria. g) Rare germaria in which germline is completely lost, encompassing 5% of germaria. This is also a subcategory of germaria with fused cysts and disrupted follicles. For all panels scale bar = 20 μm * $p < 0.05$, ** $p < 0.01$, *** $p < 0.001$, for all panels.

Figure 6: DNhe2 is necessary in the FC lineage for proper cell specification



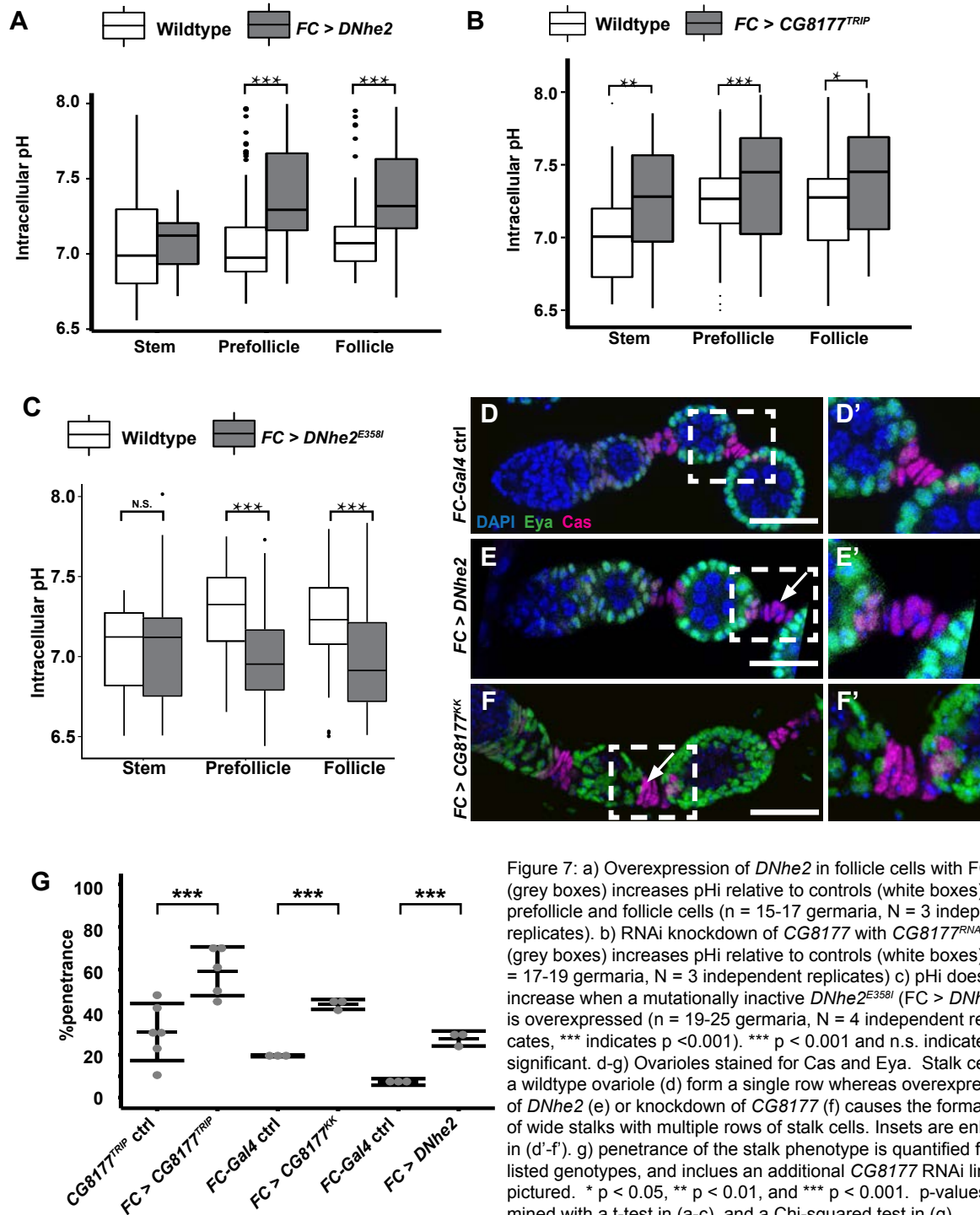
defects. I also note that in the *DNhe2^{null}* germaria, *eya* staining is less nuclear and more cytoplasmic, and the nuclei are more rounded and do not intercalate into a single row. These data confirm that the differentiation defect is largely cell autonomous and specific to the loss of *DNhe2* expression, and correlate with decreased pHi in prefollicle cells. Collectively, these phenotypes indicate that decreased pHi prevents differentiation of prefollicle cells into mature stalk cells.

Increased intracellular pH promotes excessive follicle cell differentiation

To determine whether increased in pHi affects follicle cell differentiation, I raised pHi in follicle cells using two different methods, and then confirmed that the changes in pHi correlate with a phenotype. First, I found that overexpression of *DNhe2* in follicle cells with the follicle cell specific driver significantly increased pHi by 0.3–0.35 pH units in prefollicle and follicle cells ($p < 0.001$, Fig. 7A).

Second, we also searched for additional regulators of follicle cell pHi by performing an RNAi screen through a collection of 20 candidate genes in the solute carrier (SLC) family of ion transporters that are predicted to regulate pH homeostasis. To perform this screen, germaria were stained with Castor and Eyes absent (*Eya*) antibodies to identify stalk and follicle cell populations. Slides were then examined for morphological defects and changes in *Eya* patterning. Promising candidates were screen a second time with higher replicates and fidelity. Through this approach we identified *CG8177*. *CG8177* is a putative Cl/HCO₃ exchanger, which is predicted to be an acid loader, and thus predicted to increase pHi upon knockdown. Indeed, I found that RNAi knockdown of *CG8177* using FC-gal4 significantly increased pHi by 0.4 pH units and produced a significantly increased frequency of stalks with multiple rows compared to controls (Fig. 7B, F). To confirm reliable and robust differences in pHi, I also measured pHi in a proton transport dead version of *DNhe2*, *DNhe2^{E358I}* (Grillo-Hill et al. 2015). When *DNhe2^{E358I}* is overexpressed with FC-gal4, pHi does not increase (Fig. 7C), ($n = 19-25$ germaria, $N = 4$ independent

Figure 7: pHi increases correlate with stalk differentiation defects



replicates, *** indicates $p < 0.001$).

To determine if pHi increases are correlated with specification defects, I examined the stalks of both FC-gal4 driving *DNhe2* overexpression and FC-gal4 driving CG8177 RNAi. I found that the stalks between budded follicles were enlarged, with cells accumulating in multiple rows and failing to intercalate in $29 \pm 4\%$ ($n = 113$) of ovarioles with *DNhe2* overexpression (Fig. 7D). We confirmed this differentiation phenotype in two separate CG8177 RNAi lines, and found that all three perturbations increase the frequency of penetrance of the long, wide stalks by 20-25% compared to paired controls (Fig 7G). These findings suggest that increased pHi promotes excess stalk cell differentiation.

Increased intracellular pH attenuates Hh signaling

To test whether increased pHi promotes polar and stalk cell differentiation by modulating the response to these differentiation cues, I compared the expression of Notch and Hh pathway activity reporters in prefollicle cells overexpressing *DNhe2* with FC-Gal4 to wildtype controls. Overexpression of *DNhe2* did not affect the pattern or level of expression of the Notch pathway reporter, NRE-GFP (Fig. 8). I measured Hh pathway activity with *Ptc-pelican GFP*, which has previously been shown as a robust measure of Hh activity in the follicle cell lineage (Sahai-Hernandez and Nystul 2013). In wildtype follicle cells, Hh activity is highest in the FSC and drops off rapidly. Hh is also active in escort cells, the stromal cell population that produces ligands important to both germline stem cell and follicle stem cell niche.

To quantify fluorescence intensity, I stained with GFP, to mark the reporter, FasIII, to mark follicle cell membranes, and traffic jam, which is expressed in all somatic cells. I quantified GFP intensity within follicle cells by using Imaris software to select tj+ nuclear volumes within the FasIII region (Fig. 9 A''-B''). I observed a significant decrease in Hh pathway activity in both early prefollicle cells, just downstream from the FSC niche where

Hh signaling is high, as well as in later prefollicle cells, where Hh signaling is lower (Fig 9A-C). Hh activity was lower both in early pFC (defined as the first three follicle cells in the FasIII+ region) as well as pFC (defined as the next three follicle cells in the FasIII+ region). I found that in region 3, GFP intensity wasn't high enough above background to get a clear signal, so only cells highlighted in yellow (Fig. 9 A''-B'') were quantified. As early pFC are still higher in intensity than pFC, it seems like the gradient of Hh activity is largely preserved and the difference mostly comes from an overall decrease in intensity.

To test if this level of decrease in Hh activity has functional consequences, I tested if the overexpression or knockdown of *DNhe2* could rescue or enhance Hh phenotypes. I found that overexpression of *DNhe2* suppressed the accumulation of incompletely differentiated stalk cells caused by overactivation of Hh signaling. Specifically, I found that knockdown of *ptc* by RNAi (weak) in follicle cells with FC-Gal4 caused the development of long, wide stalks in $70 \pm 2\%$ ($n = 467$) of ovarioles (Fig. 10A, D), which is consistent with published results (Forbes, Lin, et al. 1996; Tworoger et al. 1999; Chang et al. 2013a). This weaker RNAi line is Bloomington stock number 28795. Overexpression of *DNhe2* along with *ptc* RNAi (weak) partially rescued this stalk phenotype, reducing the frequency of ovarioles with long, wide stalks to $30 \pm 5\%$ ($n = 279$, Fig. 9B, D). In contrast, overexpression of *DNhe2^{E358I}*, an allele with a point mutation that prevents ion translocation (Denker et al. 2000; Grillo-Hill et al. 2015), did not increase pHi (Fig. 7C) and did not suppress the *ptc* RNAi phenotype (Fig. 10D). In addition, RNAi knockdown of *DNhe2* did not enhance the *ptc* RNAi phenotype (Fig. 10C-D). These observations indicate that increased pHi attenuates wildtype and constitutively active Hh signaling.

I also found that this effect is dosage dependent, in that when Hh signaling is further perturbed via a stronger *ptc* knockdown, the overexpression of *DNhe2* does not rescue this effect (Figure 10 E-G). The stronger *ptc* RNAi line is Bloomington stock number

55686. This is likely because in contrast to the weaker *ptc* RNAi line, total penetrance was $98\% \pm 2\%$ vs. 70% , and displayed rare phenotypes not observed in the weaker knockdown, like the formation excess cas⁺ cells that appear to form a structure that resembles a stalk (Fig 10E-F, dashed boxes and insets). Strong Hh signaling provides “gas” to accelerate the specification of cas⁺ cells, while pHi provides moderate “breaking” to stop the accelerated specification. In the context of a strong knockdown, the “gas” overwhelms the ability to “break”.

To investigate how increased pHi attenuates Hh signaling, I examined the levels of a Smoothened::*GFP* (*Smo*::*GFP*) fusion protein expressed with FC-Gal4. I found that *Smo*::*GFP* levels are highest in Region 2b, where prefollicle cell pHi is low, and decreased progressively toward Region 3, where the pHi is higher (Fig. 11A, A', E). In contrast, the level of an unrelated fusion protein, CD8::*GFP*, expressed with the same driver was uniform throughout the germarium (Fig. 11D-D'), indicating that the decrease in *Smo*::*GFP* is not due to differences in FC-Gal4 expression levels or GFP stability in these regions. To measure *Smo*::*GFP* intensity in between regions, I drew a line as indicated by the dotted lines (Fig 11 A) and took the average GFP across such a line. Prefollicle cells in Region 2b are indicated by a white line and follicle cells in Region 3 are indicated by a yellow line. In addition, I found that overexpression of wildtype *DNhe2*, but not *DNhe2*^{E358I}, significantly decreased *Smo*::*GFP* levels throughout the germarium (Fig 11 B-D, F). As *Smo*::*GFP* is expressed mostly in the membrane, to measure GFP intensity in the entire germarium, I created a mask using the FasIII channel, and then took the average GFP intensity within the FasIII⁺ region. I believe this manner of measurement accurately captures the average reduction in GFP intensity between genotypes.

Conclusions

Conclusions and speculations from *Drosophila* Data

Figure 8: Notch pathway activity is not affected by pHi

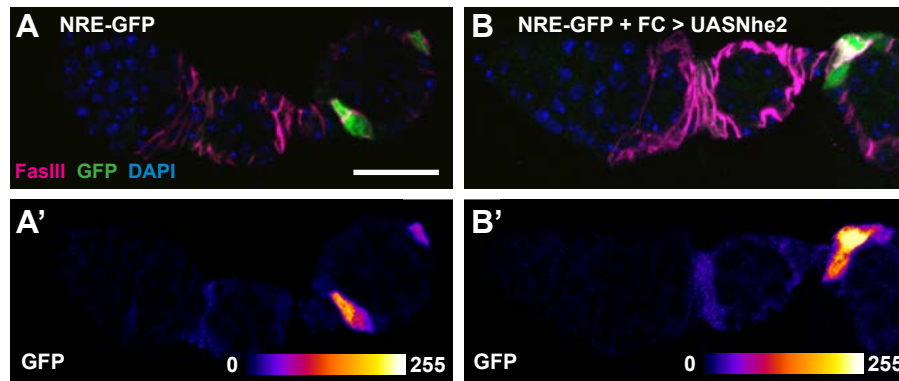


Figure 8: Germaria stained for FasIII and GFP with the Notch pathway reporter, Notch-Response-Element fused to GFP (NRE-GFP) alone (a) or in combination with *DNhe2* overexpression (b). Pseudo-colored image reflecting the intensity of the GFP channel shown in a' and b'. f) pHi does not increase when a mutationally inactive *DNhe2*^{E358I} (Grillo-Hill et al., 2015) (*FC > DNhe2*^{E358I}) is overexpressed (n = 19-25 germaria, N = 4 independent replicates, *** indicates p < 0.001).

Figure 9: Hh pathway activity decreases when pHi increases

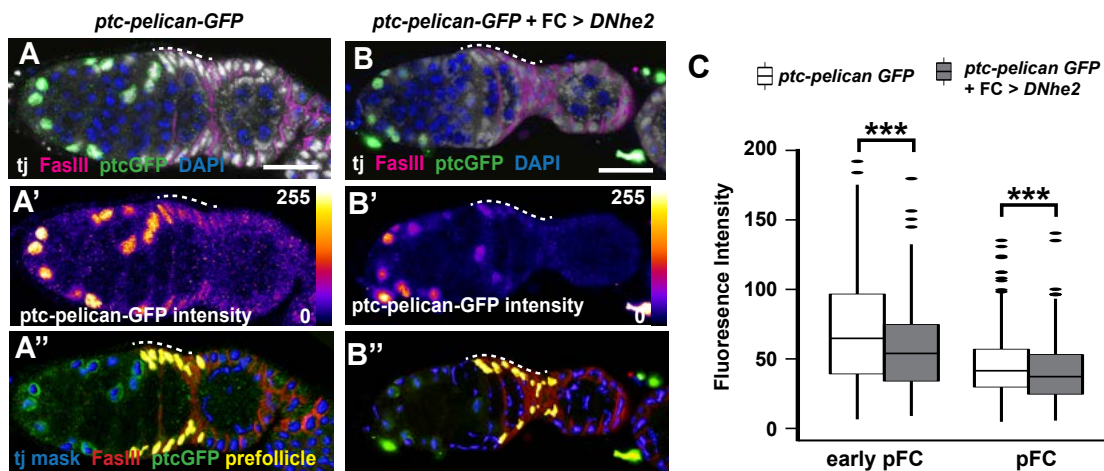


Figure 9: a-b) Germaria expressing *Ptc-pelican-GFP* only (a) or *Ptc-pelican-GFP* and *DNhe2* in follicle cells (b) were stained for GFP, FasIII to identify follicle cells, traffic jam to identify somatic cell nuclei, and DAPI. Pseudocolor of GFP channel in a' and b' reflects fluorescence intensity. Nuclear volumes selected for intensity measurements (yellow) are shown in a'' and b''. Prefollicle cell regions are indicated with white dashed lines. c) Quantification of *Ptc-pelican-GFP* fluorescence intensities in germaria expressing *Ptc-pelican-GFP* only (white boxes) or *Ptc-pelican-GFP* and *DNhe2* in follicle cells (grey boxes) in early prefollicle cells (early pFC) or prefollicle cells (pFC) (n > 450 cells for all genotypes, N = 3 independent replicates).

Collectively, these findings suggest a model in which an increase in pHi contributes to the patterning of prefollicle cell differentiation by destabilizing Smo and thus reducing the level of Hh signaling to promote the stalk cell fate (Fig. 12A). My data shows that in a wildtype stalk, a pHi gradient and Hh gradient oppose each other. When Hh activity is moderately increased through the knockdown of *ptc* RNAi, extra stalk cells that fail to intercalate form. Moderate defects are rescued by increased pHi via increasing *DNhe2* expression.

From my data, I know that overall decreased levels of smo are correlated with increased pHi, and that this regulation happens post-transcriptionally, as the *smo::GFP* is under the control of a *gal4* driver which means the expression is independent of pH. The balance between ubiquitination and phosphorylation controls is one mechanism for controlling the levels of smoothened post-transcriptionally. Ubiquitination plays a key role in regulating the sub-cellular localization of smoothened, and in particular ubiquitination is prevented by phosphorylation of the smoothened auto-inhibitory domain (SAID) and the C-terminal tail (S. Li et al. 2012).

One possible mechanism for pHi attenuation of smoothened could be shifting the likelihood of ubiquitination and subsequent degradation towards ubiquitination through interactions with the smoothened autoinhibitory domain. Another possibility is that pHi somehow interferes with the binding kinetics of CK1, PKA, or GPRK2, three kinases that serially phosphorylate the SAID.

It will be of interest to the laboratory in future work to test these mechanisms in a model more amenable to mechanistic perturbations and testing binding efficacy, like *Drosophila* S2 cells.

While these mechanistic possibilities remain speculative, this work

Figure 10: Increased pHi rescues moderately upregulated Hh activity

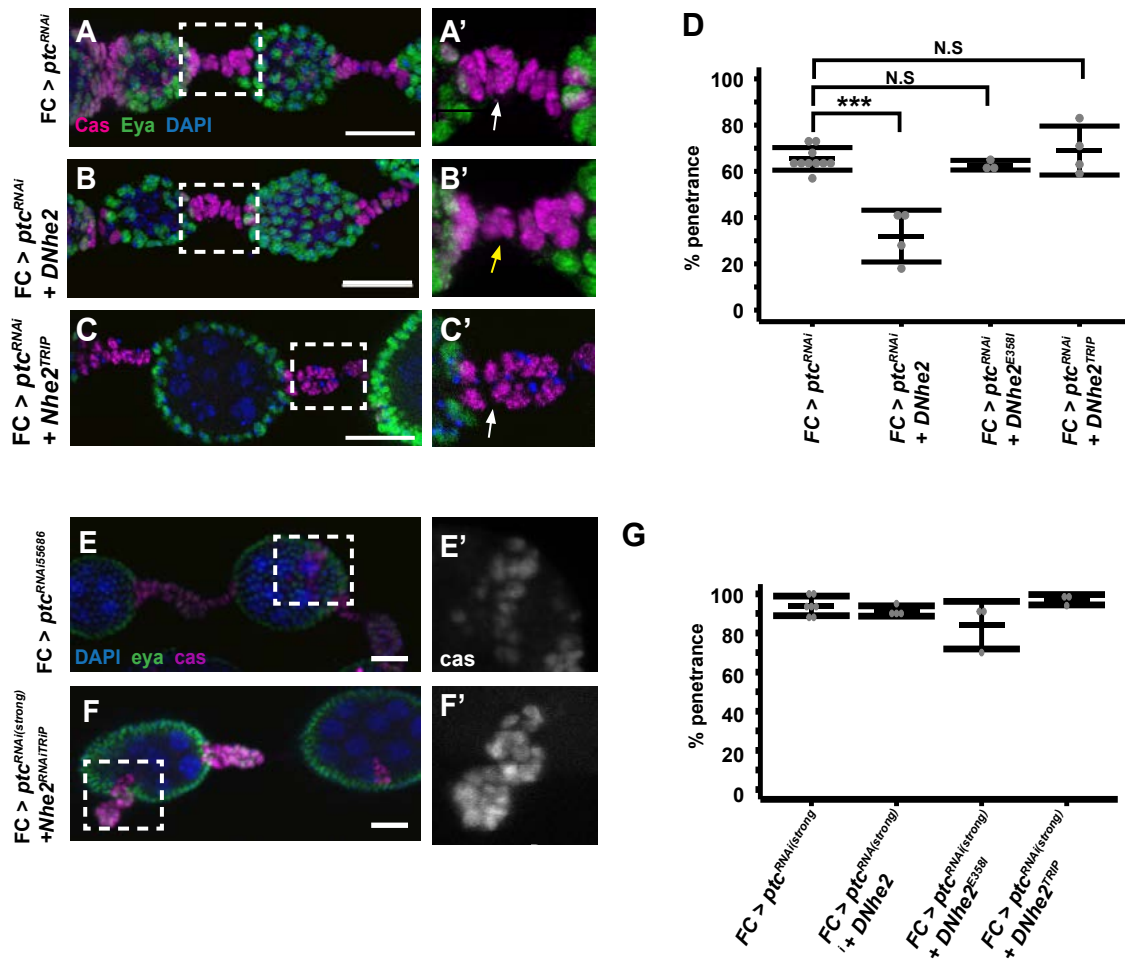


Figure 10: a-c) Ovarioles stained for Cas and Eya from $FC > ptc^{RNAi(weak)}$ (a), $FC > ptc^{RNAi(weak)} + DNhe2$ (b), and $FC > ptc^{RNAi(weak)} + DNhe2^{TRIP RNAi}$ (c). Insets enlarged in a'-c'. White and yellow arrows indicate stalks with double or single rows of cells, respectively. d) The penetrance of the stalk phenotypes in each genotype ($n > 100$ ovarioles for all genotypes, $N = 3-6$ independent replicates). e) Example of a more severe stalk formation defect from the stronger knockdown of $ptc^{RNAi(strong)}$, boxes show ectopic cas expression which appears in a small subset of germaria, and not found in the weaker knockdown. f) Example of ectopic cas cells in combination with $DNhe2^{TRIP}$. g) Penetrance of the $ptc^{RNAi(strong)}$ in combination with $FC > DNhe2$ overexpression, $DNhe2^{E358I}$ overexpression or $DNhe2$ knockdown via TRIP RNAi do not change the penetrance of the phenotype. p-values determined with a Chi-squared test, *** $p < 0.001$

demonstrate that pHi is a novel mechanism to fine-tune cell specification.

Additionally, in addition to the effects on Hedgehog signaling, it is likely that changes in pHi also modulate the activity of other pathways. Modulations in pH signaling are a way to fine tune and coordinate multiple signaling inputs, and although I did not find an effect on Notch pathway activity, it is likely other pathways are attenuated or modulated by pHi changes.

On pHi measurements and variability

Over the course of experimentation, I measured pHi in five separate experiments. I observed some variability in pHi measurements between the FSC and prefollicle and follicle cells which are summarized in Table 2. The most concerning of these is that in one out of the five pH experiments I conducted there is not a significant difference between stem and prefollicle cell, although there is still a difference between stem and follicle cells. I believe that these variations, and the lack of detection of a difference is within the range of normal statistical noise with each separate experiment representing an independent test of the true differences within populations.

Variations in measurements is a known challenge with imaging pHi in living, intact tissue, and the only other study of pHi in the *Drosophila* (Grillo-Hill et al. 2015), the measurements of pHi in eye imaginal discs varied by 0.2 pHi units. This variability has three possible sources - biological, technical, and stochastic. Biological variation could come from physiological state of the animal when the tissues are dissected, or from differences in the level of pHlourin expression [TN8]. Theoretically, the mCherry probe should minimize differences from pHlourin expression; however, if overall expression is substantially lower, some fraction of mCherry expression could fall below the limit of our detection, resulting in artificially higher absolute pH values. Indeed, the largest difference in absolute values,

Figure 11: Increased pHi decreases Smoothed levels

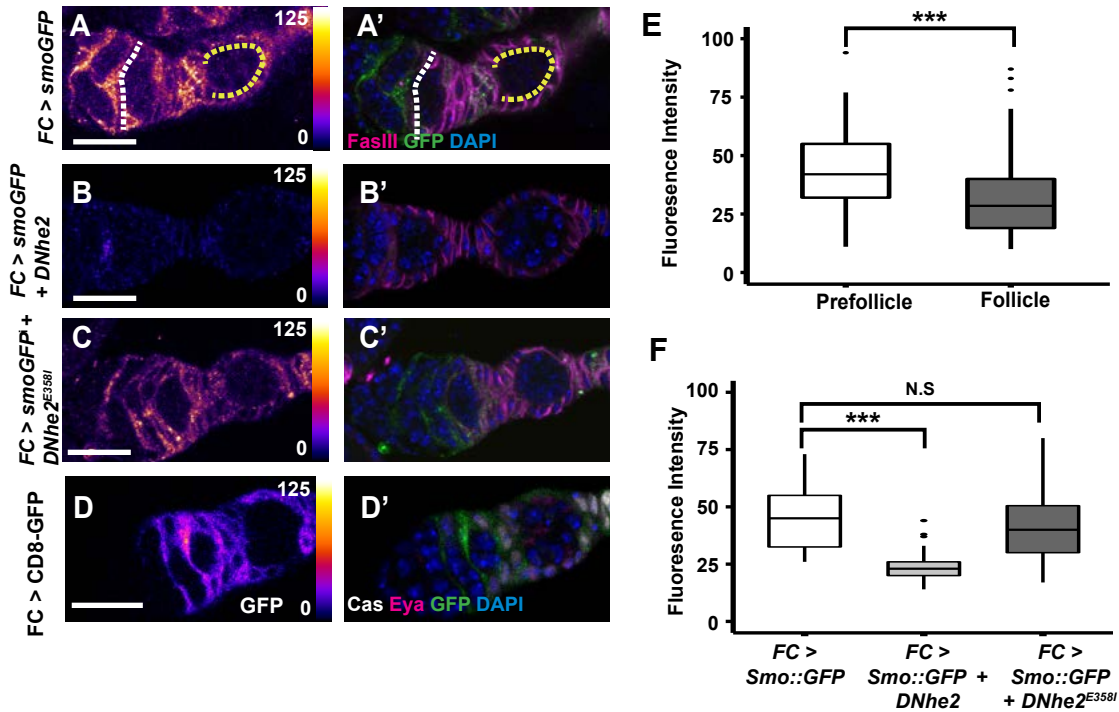


Figure 11: a-c) Ovarioles stained for GFP from FC-Gal4 driving *Smo::GFP* expression only (a), *Smo::GFP* and wildtype *DNhe2* (b), or *Smo::GFP* and *DNhe2^{E358I}* (c). In ovarioles expressing *Smo::GFP* only (a), the fluorescence intensity is higher in prefollicle cells (yellow line) than in follicle cells (white line). Co-expression of wildtype *DNhe2* (b) but not *DNhe2^{E358I}* (c) significantly reduces the intensity of the signal throughout the germarium. d) A germarium stained with Cas (grey), GFP (green), Eya (magenta), and DAPI (blue) with FC-Gal4 driving expression of *CD8::GFP*. Pseudo-colored in (d) shows uniform intensity of the GFP channel in prefollicle cells and follicle cells. e) Quantifications of the fluorescence intensity in prefollicle and follicle cell regions of germaria with FC-Gal4 driving *Smo::GFP* expression, stained for GFP (n = 31 germaria). f) Expression of *DNhe2* but not *DNhe2^{E358I}* decreases the fluorescence intensity of *Smo::GFP* (n > 29 germaria for all genotypes).

Figure 12: Model for effects of Hh and pHi on stalk formation

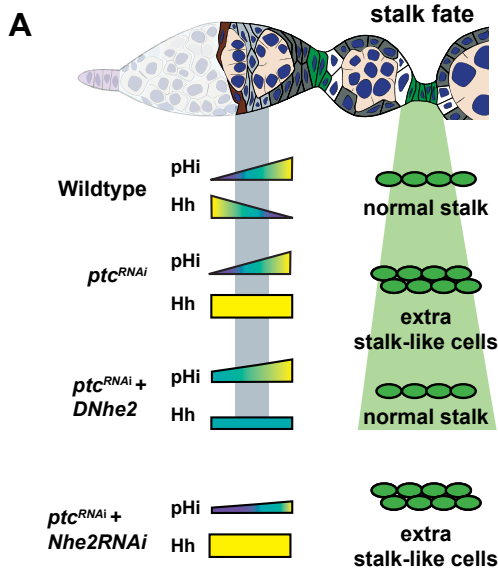


Figure 12: a) Schematic summarizing the genetic interaction between RNAi knockdown of *ptc* and overexpression of *DNhe2*. In wildtype germaria, pHi increases in prefollicle cells as Hh pathway activity decreases, and a normal stalk forms. RNAi knockdown of *ptc* results in excessive Hh signaling and the accumulation of extra stalk-like cells, as described previously. Overexpression of *DNhe2* increases pHi, attenuates Hh signaling and suppresses the stalk cell phenotype caused by RNAi knockdown of *ptc*.

between FlpOut clones between Figure 3A and 3C were conducted on tissues using different drivers to express pHLourin. As the FLPout-gal4 driver produced much stronger expression, it is likely that this difference partially accounts for the differences in absolute values; however, the differences between stem and prefollicle are similar to what we observe in the 109-30 experiments.

Technical variation could come from change in the equipment, such as those caused by upgrades to the confocal microscopes made by the core facility over the course of this study. Because of these challenges, I always prepared and imaged control samples along side every experimental sample for each replicate of every experiment, and also generated standard curves at the same time for each genotype and experimental replicate. When we compare the pHi values of FSCs, prefollicle cells and follicle cells within the same set of germaria (one “set” is comprised of three replicates, dissected and imaged on three different days), I consistently find that pHi increases with differentiation. Across the five control experiments I conducted (which were done with different microscopes over a four-year period), I find that the pHi increases by a consistent and statistically significant amount in four of the five separate experiments, which is summarized in Table 2.

A further statistical argument makes the case for the aberration in a single experiment to fall within the natural range of variation. Bayes’ Theorem predicts the probability of *detecting* an event, given the likelihood of the event. If we take the average of the p-values calculated over the course of five experiments, we find that on average our p-value is 0.13. While 0.13 seems high upon first approximation, we note that in four out of five experiments p-value is less than 0.05, and in one experiment it is 0.58. Thus, we can roughly estimate, based on the variability in our experimental method how likely it is that we would detect a difference, given a true difference in the population. This calculation assumes that the probability of a true difference is 0.87 and the probability of detecting

a true difference is also 0.87, 0.87 and multiplied by 0.87, is 0.75. This calculation is dependent on using 0.87 both the probability of the rate of detection and a probability of there being a true difference. The assumption I made in estimating this probability is that those values are the same, and that they are the average of the p-values for all experiments.

Furthermore, each individual experiment I run compounds this probability; therefore, the probability of over the course of five experiments of *always* detecting a difference is the probability of a single instantiation of the event raised to the number of events. This means that $P(\text{detection in a single experiment})^{\text{number of experiments}} = 0.75^5 = 0.25$. This means that given the variability in my data, there's only 25% chance that *all* of the data would show a true difference and a 75% chance that at least one experiment would not show a difference. Given that the 0.87 value is an estimate, I also ran the same calculations using 0.90 and 0.95 to estimate the likelihood of a true difference, and the likelihood that I would detect a true difference. These estimates give me a range of 0.25-0.60 probability of at least one experiment not showing a true difference. This means that there is somewhere between a 40-75% chance that at least one experiment would not detect a difference, given that the difference is true. Thus, I believe that the smaller difference that I observed in Fig. 3C is most likely due to normal statistical variation, and is well within the range of what I might expect to see given the variability in our data. In addition, I took a conservative approach of excluding values that fell outside the linear range of the sensor from the calculation of the means which may have resulted in an underestimation of the pHi.

mESC results

As noted in the acknowledgement, the following mESC work was done in collaboration with Diane Barber and Bree Grillo-Hill. To determine the role of pHi dynamics in the differentiation of another stem cell type, we investigated clonal mESCs (Murry and Keller 2008b; Young

Table 1

Three Point Calibration				Two Point Calibration					
	Cell Type	Intercept	Slope	r^2		Cell Type	Intercept	Slope	r^2
1	Follicle	-6.222	1.035	0.917	1	Follicle	-6.247	1.038	0.922
2	Prefollicle	-5.741	0.954	0.903	2	Prefollicle	-5.776	0.958	0.909
3	Stem	-5.785	0.954	0.852	3	Stem	-5.685	0.945	0.867

Differences Three Point vs. Two Point				
	Cell Type	Intercept	Slope	r^2
1	Follicle	0.025	-0.003	-0.005
2	Prefollicle	0.035	-0.004	-0.006
3	Stem	-0.100	0.009	-0.015

Table 1: A comparison of the slope and y-intercept values from a linear regression model show us that only very slight differences occur when using a three-point calibration curve versus a two-point calibration curve

Table 2

All pHi Experiments, Comparison of contols

Experiment	dNhe2OE	dNheRNAI	dNhe2EIOE	CG8177 RNAi	FLPoutClones
Driver	FC-gal4	FC-gal4	FC-gal4	FC-gal4	Actin-gal4
Stem pHi	7.07	6.92	7.04	7.05	6.79
Prefollicle pHi	7.10	7.14	7.27	7.22	7.03
Follicle Cell pHi	7.17	7.09	7.24	7.25	7.27
$\Delta pHi(Stem vs. Prefollicle)$	0.03	0.21	0.23	0.17	0.25
p-value for Stem vs. Prefollicle	0.58	3.83×10^{-3}	0.01	0.04	4.85×10^{-5}
$\Delta pHi(Stem vs. Follicle)$	0.11	0.17	0.20	0.21	0.48
p-value (Stem vs. Follicle)	0.06	1.06×10^{-3}	0.03	0.01	3.03×10^{-13}
n(germaria)	20	16	19	17	36

Table 2: While there are differences of about 0.2 pHi units in absolute pHi values calculated across experiments, with the exception of a single experiment, the difference between stem and prefollicle and stem and follicle holds remarkably steady at close to 0.2 pH units. From this, we can tell that differences of 0.2 pH units also are reliably significant across experiments and cell types, demonstrating the methodology is sufficient to detect differences of that magnitude.

2011) derived from the inner cell mass of blastocyst embryos. Clonal mESCs maintain pluripotency when cultured with leukemia inhibitory factor (LIF) and inhibitors of mitogen-activated protein kinase (MEK) and glycogen synthase kinase-3 β (2i) but spontaneously differentiate when LIF/2i is removed and, after 3 to 5 days, acquire markers of primed epiblast stem cells (epiSCs). The addition of the 2i cocktail of inhibitors results in a more homogenous culture more reflective of the earliest stages of differentiation (Q.-L. Ying et al. 2008). Using cells loaded with the pH sensitive fluorescent dye BCECF (Grillo-Hill et al. 2015), we found that pHi increased during the first 72 hours of mESC differentiation. Over 6 days, naïve mESCs retained a near constant pHi between 7.40 ± 0.06 and 7.46 ± 0.07 , but in differentiating cells there was a transient increase in pHi to 7.65 ± 0.06 at 48 hours and 7.57 ± 0.05 at 72 hours ($p < 0.001$, Fig. 13A), with pHi returning to values similar to undifferentiated cells at 96 hours and 6 days.

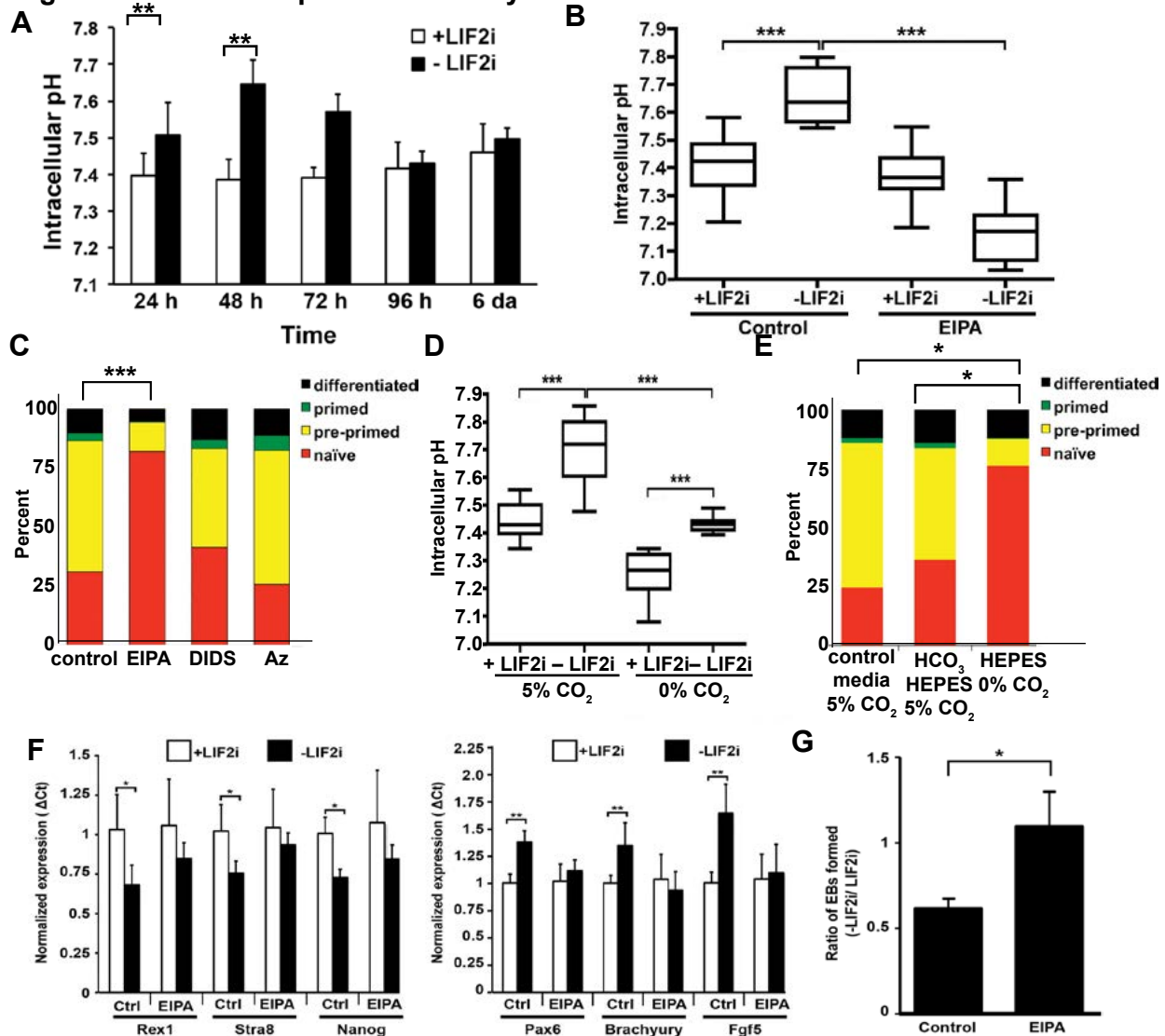
Because MEK, a component of the 2i cocktail of inhibitors that homogenizes mESC population also increases activity of NHE1, (Malo, Li, and Fliegel 2007), which could increase pHi, we tested whether the higher pHi we observed with removing LIF/2i was merely because MEK was no longer inhibited. However, when we adapted self-renewing cells to LIF without 2i, we observed a similar increase in pHi upon differentiation at 72 hours, indicating that the increased pHi does not merely reflect removal of MEK inhibition of NHE1 (Fig. 14A).

We next asked whether inhibiting NHE1 with the selective pharmacological inhibitor 5-(N-ethyl-N-isopropyl) amiloride (EIPA) changed pHi in the absence or presence of LIF/2i. In self-renewing naïve cells maintained with LIF/2i, pHi was not different in the absence and presence of EIPA (Fig. 13B). However, with EIPA, pHi did not increase with removal of LIF/2i for 72 hours and was significantly lower than in control naïve cells, possibly reflecting loss of proton efflux of metabolic acids generated by increased glycolysis that

occurs with differentiation (Ge et al. 2010).

Although NHE1 activity was previously shown to be necessary for differentiation of mESCs to cardiomyocytes (X. Li et al. 2009), to our knowledge, a role for increased pHi in spontaneous differentiation of mESCs to epiSCs has not been reported. Thus, we determined the differentiation state of mESCs in the absence and presence of EIPA using several approaches. We first used a dual-reporter mESC cell line expressing developmentally regulated miRNA clusters that are tagged with distinct fluorophores (Parchem et al. 2014). In this reporter line, naïve mESCs express *mir-290-mCherry*, but not *mir-302-eGFP*; “pre-primed” cells in intermediate stages express both reporters; primed epiSCs express *mir-302-eGFP*, but not *mir-290-mCherry*; and both reporters are silenced in cells that have differentiated further. FACS analysis showed that EIPA had no effect on the proportion of naïve (*mir-290-mCherry*⁺, *mir-302-eGFP*⁻) cells in self-renewing +LIF2i medium (Fig. 14B). However, after 72 hours without LIF2i there was a significantly higher percentage (82.0%) of naïve cells (*mir-290-mCherry*⁺, *mir-302-eGFP*⁻) with EIPA compared with controls (30.9%; $p < 0.001$) (Fig. 13C). Additionally, imaging cells at 5 days without LIF2i showed that most control cells expressed *mir-302-GFP*, but with EIPA, most cells retained expression of *mir-290-mCherry* (Fig. 14C), indicating more cells in a predominantly naïve state with EIPA. We found no increase in cell death with EIPA treatment (Fig 14D), indicating that attenuated differentiation is not due to selective elimination of pre-primed and/or primed cells. In contrast to attenuated differentiation with EIPA, FACS analysis indicated that differentiation with the pharmacological inhibitors 4,4'-Diisothiocyano-2,2'-stilbenedisulfonic acid (DIDS), which blocks activity of anion exchangers, or acetazolamide (Az), which blocks carbonic anhydrases, was not different than control (Fig. 4C). Moreover, despite the efficacy of both inhibitors in attenuating pHi recovery when cells were rapidly switched from a HCO₃⁻ free, HEPES buffer at 0% CO₂ to a HEPES-free buffer containing 25 mM NaHCO₃ superfused with 5% CO₂ (Fig 14E),

Figure 13: Increased pHi is necessary for mESC differentiation



a) Figure 13: pHi measurements show significant change at 48 and 72 h after removing LIF2i. Data are means \pm s.e.m. of 3 cell preparations. b) The NHE1 inhibitor EIPA blocked the increase in pHi seen in control cells cultured without LIF2i. Data are values at 72 h in 5 cell preparations. c) In the dual-reporter mESC reporter line, naïve mESCs expressed mir-290-mCherry (red); cells in intermediate stages, termed pre-primed, expressed both mir-290-mCherry and mir-302-eGFP (yellow); primed epiblast stem cell (epiSC) cells expressed mir-302-eGFP (green); and further differentiated cells have silenced both reporters (black). After 72 h cultured without LIF2i, 30.9% of control cells express mir-290-mCherry alone. This is significantly increased when cells are treated with EIPA to 82.0% (n=6 independent cell preparations). d) Cells maintained in HEPES-buffered DMEM in the absence of CO₂ had lower pHi in the presence and absence of LIF2i compared with cells maintained at 5% CO₂. Data are means of values at 72 h in 4 cell preparations. e) In the dual-reporter mESC reporter line, more cells maintained in HEPES-buffered DMEM in the absence of CO₂ expressed the naïve cell miRNA mir-290-mCherry (75.4%, red) compared to cells maintained at 5% CO₂ in either a predominantly-HEPES buffered DMEM (36.4%) or control DMEM (24.6%) (n=3 independent cell preparations). f) qRT-PCR analysis of pluripotency genes showed that control cells cultured without LIF2i for 72 h downregulated Rex1, Stra8 and Nanog. Expression of these pluripotency markers is retained with EIPA treatment (no significant differences detected by Student's t-test). Expression of differentiation genes Pax6, brachyury and Fgf5 increased with control cells after 72 h without LIF2i. With EIPA treatment, cells cultured without LIF2i for 72 h do not show upregulation of these genes (no significant differences detected by Student's t-test). g) EIPA treatment maintains functional pluripotency as measured by embryoid body (EB) formation. The number of EBs formed after for 72 h without LIF2i was normalized to the number of EBs formed in naïve mESCs for each experiment. Control mESCs form fewer EBs than naïve mESCs (61 \pm 5%). However, mESCs grown without LIF2i but with EIPA for 72 h form EBs as well as naïve mESCs (109 \pm 20%, p<0.05). (mean \pm standard deviation; n = 130-150 droplets; N = 3 independent experiments). For all panels, * p < 0.05, ** p < 0.01, *** p < 0.001 by t-test.

neither inhibitor prevented the increase in pHi with differentiation (Fig 14F).

To confirm that attenuated differentiation was due to decreased pHi rather than inhibiting a function of NHE1 independent of proton efflux we maintained in a predominantly HEPES-buffered medium at 5% and 0% CO₂. In the experiments measuring pH and testing the effect of EIPA on differentiation, cells were maintained in a predominantly NaHCO₃ buffered medium, which is toxic to cells in a low CO₂ condition. To test the effect of CO₂, it was necessary to confirm that changing buffering components did not affect pHi or differentiation. Indeed we found that the pHi and differentiation of cells maintained at 5% CO₂ in DMEM containing 5 mM NaHCO₃ and 30 mM HEPES and HEPES-buffered medium containing 5 mM NaHCO₃ was not different than cells maintained at 5% CO₂ in control medium containing 44 mM NaHCO₃ and no HEPES (Fig. 13D-E). In contrast, cells maintained at 0% CO₂ in a HEPES-buffered medium lacking NaHCO₃ had a lower pHi with LIF2i and although pHi was increased after 72 h without LIF2i, it was significantly lower than controls without LIF2i and similar to controls with LIF2i (Fig. 4D). Additionally, FACS analysis of dual-reporter cells showed that differentiation of cells maintained at 0% CO₂ was significantly attenuated, with 76% *mir-290-mCherry*⁺, *mir-302-eGFP*⁻ compared with 24% and 36% *mir-290-mCherry*⁺, *mir-302-eGFP*⁻ with cells maintained at 5% CO₂ (Fig. 4E). Together, these data indicate that an increase in pHi, likely to greater than pHi 7.5, is necessary for mESCs to differentiate toward the epiSC fate.

For a second approach to determine the differentiation state of mESCs in the absence and presence of EIPA we used qRT-PCR to quantify expression of pluripotency and differentiation markers. For control cells, we found that removal of LIF2i for 72 hours decreased expression of mESC markers Rex1, Stra8, and Nanog, and increased expression of epiblast markers Fgf5, brachyury (T) and Pax6, as expected (Parchem et al. 2014). In contrast, we observed no significant changes in the expression of these

genes upon removal of LIF2i in cultures treated with EIPA (Fig. 13F), indicating the increase in pHi is required for expression of genes that drive differentiation. To determine functional pluripotency in EIPA-treated cells cultured without LIF2i we tested for the formation of embryoid bodies (EBs), which form spontaneously when mESCs are grown in suspension (Kurosawa 2007). We grew mESCs with or without LIF2i and EIPA for 72 hours, and then plated cells in suspension as described (Kurosawa 2007). We found that control cells grown without LIF2i for 72 hours formed EBs at a lower frequency than control cells grown with LIF2i ($61 \pm 5\%$) (Fig. 14G). However, after 72 hours without LIF2i, cells treated with EIPA formed EBs at a significantly higher frequency than control cells ($109 \pm 20\%$, $p < 0.05$), suggesting that mESCs treated with EIPA maintain functional pluripotency even in the absence of LIF2i.

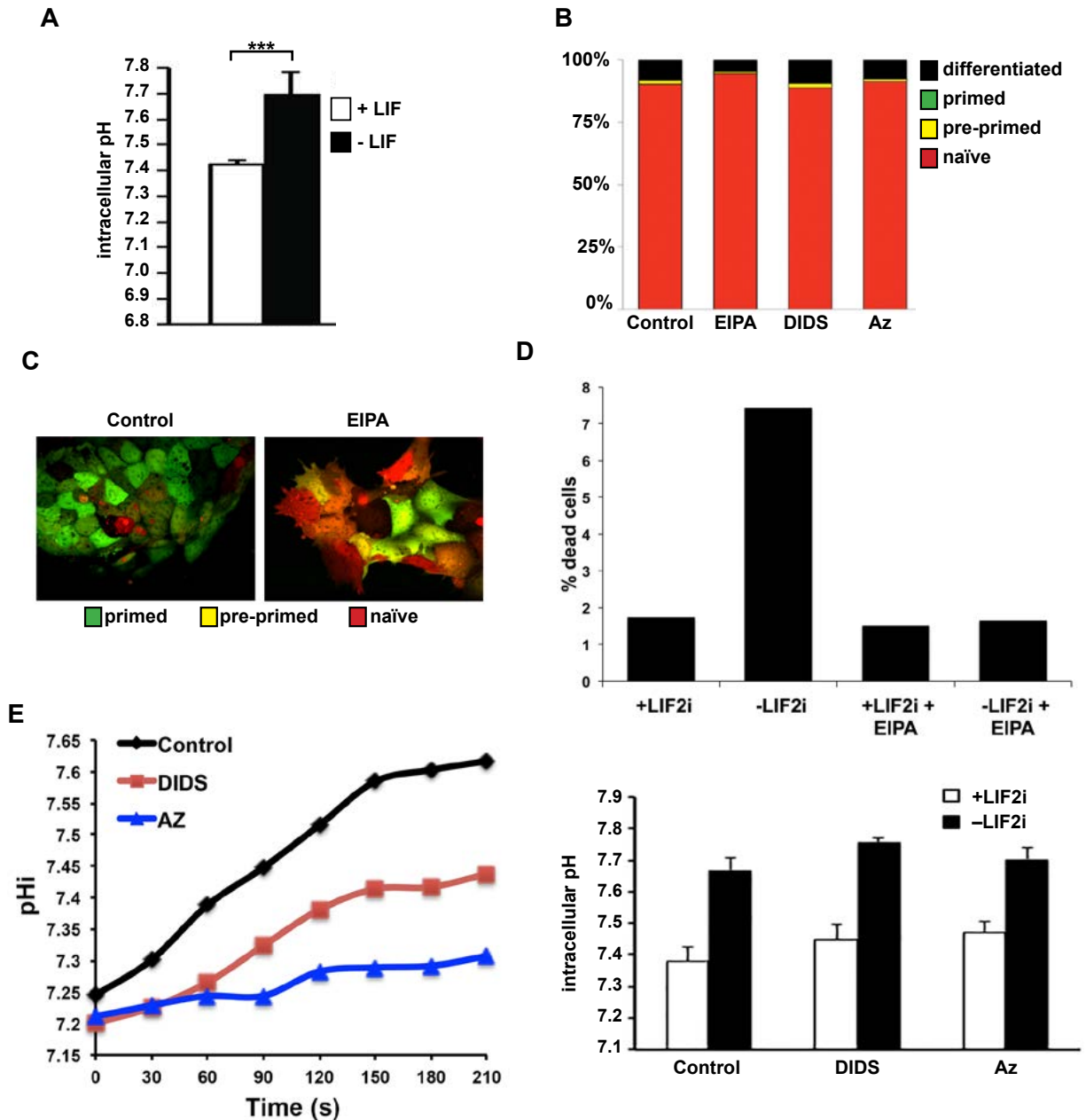
These results demonstrate that in two separate systems pHi can impact differentiation. I believe this represents a novel and substantial increase in our knowledge of the workings of stem cell differentiation beyond what has previously been described.

Methods:

pHluorin quantitative imaging

FLPout clones were generated with a 15-30 minute heat shock at 37°C and dissected 7-10 days post clone induction. In FSC clones, FSCs can be identified as the anterior-most cell in the clone (Margolis and Spradling 1995; Nystul and Spradling 2007), prefollicle cells are found just downstream from the FSCs, in Region 2b, and more mature follicle cells are located further downstream, in Region 3 of the germarium. For expressing UAS-mCherry::pHluorin with a follicle cell specific (FC) driver (109-30-Gal4), flies were dissected 7 days post eclosion. The chambers that flies were imaged in were custom 3-D printed chambers made to the size of 22 x 40 mM coverslip. To image, I made a sealed chamber by adding a thin coating of vacuum grease to the bottom of the chamber, and

Figure 14: mESC differentiation effects are specific to Nhe1



a) Cells maintained for two weeks in LIF (without 2i) have increased pH_i 48 h after LIF removal. b) The proportion of naïve (mir-290-mCherry⁺, mir-302-eGFP⁻) dual-reporter cells cultured with LIF2i was not different in the presence of EIPA, DIDS or acetazolamide (AZ) compared with controls. c) Images of dual-reporter cells maintained without LIF2i for 5 days show that more cells express mir-290-mCherry⁺ in the presence compared with the absence of EIPA. d) Cell death was measured by flow cytometry showing increased DAPI. The percentage of dead cells increased with removal of LIF2i (1.7% to 7.4%), but did not change with EIPA treatment (1.5% with LIF2i, 1.6% without LIF2i). (n=2 independent cell preparations). e) DIDS and acetazolamide attenuate pH_i recovery after rapidly switching cells from a nominally HCO₃-free HEPES buffer at 0% CO₂ to a HEPES-free buffer containing 25 mM NaHCO₃ superfused with 5% CO₂. f) The pH_i of cells maintained for 72 h with and without LIF2i was not different in the presence of DIDS or acetazolamide (AZ) compared with controls.

sealed with a 22 x 50 mM coverslip.

For pHi imaging, ovaries were dissected into bicarbonate buffer as described (Grillo-Hill et al. 2015; Grillo-Hill, Webb, and Barber 2014) with 0.25 mg/mL Concanavalin A conjugated to Alexa Fluor 647 and incubated for 15 minutes prior to imaging to visualize cell membranes (Life Technologies, C21421). After dissection, I transferred ovaries into the imaging chamber with forceps, and then carefully separated individual ovarioles and removed larger late-stage egg chambers. I then added two drops of nail polish to a 12 mm coverslip and mounted the coverslip over the ovarioles to prevent them from moving.

I filled the imaging chambers with enough buffer to completely fill the well, from 500 μ L to 1 mL. To calibrate mCherry::pHluorin ratios to pHi values for each experiment and genotype, fresh ovaries were equilibrated into nigericin buffer pH 6.5 or 7.5 for 15 minutes prior to imaging as described (Grillo-Hill et al. 2015; Grillo-Hill, Webb, and Barber 2014) using 40 μ M nigericin (Invitrogen, N1495). 16-bit images in 1024 x 1024 format were acquired on a Leica SP5 or Leica SP8 laser scanning confocal with gain, laser power, pinhole size and other image acquisition settings consistent across matched control and experimental conditions.

To obtain fluorescence intensity measurement, I first subtracted background using a large ROI in a black area of the image. Then, ROIs were drawn around individual cells using the ConcanavalinA-647 dye as a guide to outline individual cells. I measured one to two stem cells and three to five prefollicle and follicle cells of bright and uniform intensity and selected the most highly expressed cells for measurement. Each ROI was measured in one or two slices of 1 μ M. If two slices were used, fluorescence intensity was averaged over two slices. Calibration curves for each experiment, genotype, and cell type were generated and linear regression analysis yielding r^2 values of at least 0.70 were obtained

and used to calculate pHi values from ratios.

Drosophila tissue immunofluorescence staining

Unless otherwise noted, ovaries were fixed and stained according to previously published immunostaining protocols (Castanieto, Johnston, and Nystul 2014). To reduce background in ovarioles stained for Cas and Eya, ovaries were blocked in 0.5% BSA (Sigma, A7979) in PBST (PBS + 0.2% Triton X-100) for at least 1 hour prior to addition of both primary and secondary antibodies.

The following antibodies were used: from Developmental Studies Hybridoma Bank (Iowa City, Iowa); mouse anti-eya (eya-10H6, 1:50) mouse anti-Fasciclin III, (7G10, 1:100); guinea pig anti-traffic jam (1:1000) (a gift from Allan Spradling); from Life Technologies (A11122) rabbit anti-GFP (1:1000); from Santa-Cruz Biotechnologies (Santa Cruz, CA) rabbit anti-vasa (1:1000), rabbit anti-castor (1:4000 or 1:5000) (a gift from Ward Odenwald). The following secondary antibodies were used at 1:1000: anti-mouse Alexa-Fluor 488 and 555 (Invitrogen A11001, A21422), anti-rabbit Alexa-Fluor 488 and 555 (Invitrogen A11008, A21428), and anti-guinea pig Alexa-Fluor 633 (Invitrogen, A21105). Images were acquired on a Leica SP5 or SP8 line-scanning confocal for all experiments in which quantitative fluorescence comparisons were made and determination of presence or absence of Eya. A Zeiss M2 Axioimager with Apotome unit for images in which comparisons of morphological features were made. Images were cropped, rotated and contrast adjusted in Adobe Photoshop and saved as .tif files.

Quantitative Microscopy: *Ptc-pelican-GFP quantitative analysis*

The middle section of a germarium varying in thickness from 1 to 5 μM stained with tj, FasIII, GFP and DAPI were imaged on a Leica SP5 inverted confocal. Imaris 3D analysis software (Bitplane) was used to render 3D surfaces over tj expressing in all somatic cell nuclei. Prefollicle cells were then manually identified and selected based on the position and intensity of FasIII staining. Mean *Ptc-pelican-GFP* intensity per nuclear volume

was measured with the Imaris software. Three independent experiments all had similar distributions, means and standard deviations, so data were aggregated.

Egg laying assays

Flies eclosed within 48 hours were moved into egg-lay vessels. Egg laying vessels consist of standard plastic polypropylene fly bottles turned upside down onto standard fly food mixed with 1-3 drops of Methylene blue dye with a small amount of wet yeast. 1-3 females per bottle were left overnight, up to 20 hours, and then eggs were counted. To calculate eggs/day, I calculated an hourly per fly egg laying rate and then multiplied by 24 hours to get the average number of eggs/day/fly.

Quantitative Microscopy for Smo::GFP quantitative analysis

The middle section (1-5 slices 1 μ M thick) of a germarium stained with GFP and FasIII was imaged on a Leica SP8 inverted confocal. Two different types of quantitative analyses were performed. First, for control (109-30-gal4 > Smo::GFP), I quantified background subtracted fluorescence intensity for prefollicle and follicle cells. For each of these regions two or three lines were drawn through the brightest portion of the region, and the mean intensity of the line was measured. For the second quantification, I used the FasIII channel to mask the GFP channel, and then took a measurement of the mean fluorescence intensity within each germaria to get a measurement of the total fluorescence intensity in every germaria.

Plotting and Statistics

I used RStudio statistical analysis software to generate plots. For the boxplots displaying the pH data and the quantitative fluorescence measurements, the box represents the interquartile range (IQR) which is the middle 50% of the data. The black line is the median, and the whiskers show the range of the data, with outliers of 1.5 times the IQR plotted as dots. For the dot plots, the lines indicate the median and the standard deviation. I

believe that displaying our data thusly gives the reader the most accurate picture of the full variation within our data. Unless otherwise noted, I used RStudio to perform statistical comparisons and generate plots. The scripts used to generate plots can be found in the Appendices.

Stocks

Stocks were generated with standard crossing schemes and maintained on standard molasses food and cultured at 25°C unless otherwise noted, and all stocks were acquired from the Bloomington *Drosophila* Stock Center, unless otherwise noted.

For mCherry::pHluorin clones using FLpout system

y[1] w[*]; P{w[+mC]=GAL4-Act5C(FRT.CD2).P}S, (Bloomington ID: 4780)

For ptcRNAi experiments *ptc^{RNAi} (weak)* is a transgenic RNAi line from the TRiP collection, (y[1] v[1]; P{y[+7.7] v[+1.8]=TRiP.JF03223}attP2, Bloomington ID: 28795)

ptc^{RNAi} (strong) is a transgenic RNAi line from the TRiP collection, (y[1] sc[*] v[1]; P{y[+7.7] v[+1.8]=TRiP.HMC03872}attP40, Bloomington ID: 55686)

All experiments using FC> refers to y¹ w⁺; P{GawB}109-30 /CyO (Bloomington ID: 7023)

DNhe2 knockdown via RNAi *DNhe2^{KK102518}* is a transgenic line containing P{KK102518} (from Vienna *Drosophila* Resource Center, FlyBaseID FBti0117476) , *DNhe2^{HMC03243}* is a transgenic line from the TRiP collection (y¹ v¹; P{TRiP.HMC03243}attP2, Bloomington ID: 51491)

DNhe2 and UAS-mCherry::pHluorin: *UAS-DNhe2*, *UAS-DNhe2^{E358I}*, *DNhe2^{null}* and *UAS-mCherry::pHluorin* were as described in(Grillo-Hill et al. 2015).

CG8177 knockdown via RNAi

CG8177^{TRIP} refers to y[1] v[1]; P{y[+7.7] v[+1.8]=TRiP.HMC03399}attP40 (Bloomington ID: 51827)

CG8177^{KK} refers to P{KK100095}VIE-260B (Bloomington ID: v109594, obtained from

Vienna *Drosophila* Resource Center)

For Smo::GFP analysis: $y[1] w[*]; P\{w[+mC]=UAS-smo.GFP\}2$, (Bloomington ID: 44624)

For *Ptc-pelican GFP* analysis: yw^* ; *Ptc-pelicanGFP*, (from Tom Kornberg, University of California, San Francisco)

Mouse Embryonic Stem Cell Culture

Wild type v6.5 and dual-reporter mESCs were a generous gift from R. Blelloch (University of California San Francisco). Cells were maintained as reported (Parchem et al. 2014).

For differentiation assays, cells were plated in DMEM medium (Gibco, catalog #10569) containing Leukemia Inhibitory Factor (LIF, Millipore, #ESGRO), and inhibitors for mitogen-activated protein kinase kinase (PD0325901, Stemgent, 04-0006-10) and glycogen synthase kinase-3 β (CHIR99021, Stemgent, 04-0004-10), termed LIF2i; 24 h after plating, spontaneous differentiation was initiated by washing cells 3X in PBS and then maintaining cells for the indicated times in DMEM without LIF2i.

FACS analysis of dual-reporter mESCs was performed at the UCSF Flow Cytometry Core on an LSR II (BD Biosciences) and analysis was performed using FACSDiva software. pHi was measured as described (Grillo-Hill et al. 2015). Pharmacological inhibitors were added 24 h after plating and included 5-(N-Ethyl-N-isopropyl) amiloride (EIPA, Enzo catalog #ALX-550-266-M005, final concentration 10uM); 4,4'-Diisothiocyanostilbene-2,2'-disulfonic Acid (DIDS, Millipore catalog #309795, final concentration 1uM); acetazolamide (Sigma, catalog # A6011; final concentration 200 mM).

The efficacy of DIDS and acetazolamide was confirmed by their ability to inhibit pHi recovery after rapidly switching cells from a nominally HCO₃-free HEPES buffer at 0% CO₂ to a HEPES-free buffer containing 25 mM NaHCO₃ superfused with 5% CO₂, as previously described (Hulikova et al. 2014). For experiments with altered CO₂ and medium

NaHCO₃, cells were plated and maintained in control DMEM for 24 h, washed, and then maintained for 72 h in the absence or presence of LIF2i in NaHCO₃-free DMEM (Sigma, D5030) supplemented with glucose (4.5 g/l), HEPES pH 7.4 (30 mM), Na-pyruvate (0.11 mg/l), Glutamax (Gibco 35050-061, 1x), non-essential amino acids (1x), glutamine (2 mM), penicillin/streptomycin (100 mg/L) and fetal bovine serum (15%). Medium for cells maintained at 5% CO₂ but not for cells maintained at 0% CO₂ was also supplemented with 5 mM NaHCO₃.

To make embryoid bodies, cells were plated and differentiated as described (Kurosawa 2007) with or without EIPA for 72 h, then plated into hanging droplets (10⁴ cells per droplet) per experiment per condition in media without LIF2i on the lids of 10 cm petri dishes. Hanging droplets were cultured for 72 h. Droplets were washed in media without LIF2i to low-adhesion 6-well cell culture dishes and the number of EBs were counted the next day. Data are reported as the percentage of EBs formed, calculated by dividing the number of EBs formed by cells cultured without LIF2i by the number of EBs formed in control cells maintained in media with LIF2i. EB data reported are from three independent cell preparations with the following numbers of droplets per condition: control +LIF2i (150), control -LIF2i (150), EIPA +LIF2i (132), EIPA -LIF2i (141). Data were analyzed and statistical analysis performed in Microsoft Excel using a paired t-test.

qRT-PCR experiments

Following differentiation for 72 h, RNA was extracted from cells using Trizol (Ambion, manufacturer's protocol with the following modifications: 800 μL Trizol added to cells, 2 μL glycoblue (Ambion, [AM9515](#)) was added to visualize RNA pellet, and pellet rinsed in 75% EtOH. RNA purity was assessed on a Nanodrop spectrometer.

cDNA was synthesized using Superscript III kit (Invitrogen, 18080093) from 2 mg of RNA and diluted 1:1 before being added to the PCR reaction. Primers as described

in (Parchem et al. 2014). qPCR was performed with SYBR Greener (qPCR SuperMix for ABI prism, Invitrogen 11760) according to manufacturer's protocol on an Applied Biosystems Real-Time PCR ViiA7 instrument. qPCR analysis was done in the open-source RStudio software using the ReadqPCR and NormqPCR(Perkins et al. 2012) open-source packages available on the Bioconductor site (www.bioconductor.org). For each gene, 3-5 independent cell preparations were used.

References

- Adam, Jennifer C., and Denise J. Montell. 2004. "A Role for Extra Macrochaetae Downstream of Notch in Follicle Cell Differentiation." *Development* 131 (23): 5971–80.
- Apionishev, Sergey, Natalya M. Katanayeva, Steven A. Marks, Daniel Kalderon, and Andrew Tomlinson. 2005. "Drosophila Smoothed Phosphorylation Sites Essential for Hedgehog Signal Transduction." *Nature Cell Biology* 7 (1): 86–92.
- Assa-Kunik, Efrat, Isabel L. Torres, Eyal D. Schejter, Daniel St Johnston, and Ben-Zion Shilo. 2007. "Drosophila Follicle Cells Are Patterned by Multiple Levels of Notch Signaling and Antagonism between the Notch and JAK/STAT Pathways." *Development* 134 (6): 1161–69.
- Bai, Jianwu, and Denise Montell. 2002. "Eyes Absent, a Key Repressor of Polar Cell Fate during Drosophila Oogenesis." *Development* 129 (23): 5377–88.
- Beg, Asim A., Glen G. Ernstom, Paola Nix, M. Wayne Davis, and Erik M. Jorgensen. 2008. "Protons Act as a Transmitter for Muscle Contraction in *C. Elegans*." *Cell* 132 (1): 149–60.
- Besse, Florence, Denise Busson, and Anne-Marie Pret. 2002. "Fused-Dependent Hedgehog Signal Transduction Is Required for Somatic Cell Differentiation during Drosophila Egg Chamber Formation." *Development* 129 (17): 4111–24.
- Castanieto, Angela, Michael J. Johnston, and Todd G. Nystul. 2014. "EGFR Signaling

Promotes the Identity of Drosophila Follicle Stem Cells via Maintenance of Partial Cell Polarity.” *eLife* 3. doi:10.7554/eLife.04437.

Chang, Yu-Chiuan, Anna C-C Jang, Cheng-Han Lin, and Denise J. Montell. 2013a.

“Castor Is Required for Hedgehog-Dependent Cell-Fate Specification and Follicle Stem Cell Maintenance in Drosophila Oogenesis.” *Proceedings of the National Academy of Sciences of the United States of America* 110 (19). Am Thoracic Soc: E1734–42.

Chang, Yu-Chiuan, Anna C. Jang, Cheng-Han Lin, and Denise J. Montell. 2013b.

“Castor Is Required for Hedgehog-Dependent Cell-Fate Specification and Follicle Stem Cell Maintenance in Drosophila Oogenesis.” doi:10.1073/pnas.1300725110/-/DCSupplemental. www.pnas.org/cgi/doi/10.1073/pnas.1300725110.

Chen, Yongbin, Shuang Li, Chao Tong, Yun Zhao, Bing Wang, Yajuan Liu, Jianhang

Jia, and Jin Jiang. 2010. “G Protein-Coupled Receptor Kinase 2 Promotes High-Level Hedgehog Signaling by Regulating the Active State of Smo through Kinase-Dependent and Kinase-Independent Mechanisms in Drosophila.” *Genes & Development* 24 (18): 2054–67.

Choi, Chang Hoon, Bradley a. Webb, Michael S. Chimenti, Matthew P. Jacobson,

and Diane L. Barber. 2013. “pH Sensing by FAK-His58 Regulates Focal Adhesion Remodeling.” *The Journal of Cell Biology* 202 (6): 849–59.

Choi, Chang-Hoon, Bradley A. Webb, Michael S. Chimenti, Matthew P. Jacobson,

and Diane L. Barber. 2013. “pH Sensing by FAK-His58 Regulates Focal Adhesion Remodeling.” *The Journal of Cell Biology* 202 (6): 849–59.

Deng, Hansong, Akos A. Gerencser, and Heinrich Jasper. 2015. “Signal Integration by

Ca(2+) Regulates Intestinal Stem-Cell Activity.” *Nature* 528 (7581): 212–17.

Denker, S. P., D. C. Huang, J. Orlowski, H. Furthmayr, and D. L. Barber. 2000. “Direct

Binding of the Na⁺-H Exchanger NHE1 to ERM Proteins Regulates the Cortical Cytoskeleton and Cell Shape Independently of H(+) Translocation.” *Molecular Cell* 6

(6): 1425–36.

- Dye, Briana R., David R. Hill, Michael A. H. Ferguson, Yu-Hwai Tsai, Melinda S. Nagy, Rachel Dyal, James M. Wells, et al. 2015. “In Vitro Generation of Human Pluripotent Stem Cell Derived Lung Organoids.” *eLife* 4 (March). doi:10.7554/eLife.05098.
- Forbes, A. J., H. Lin, P. W. Ingham, and A. C. Spradling. 1996. “Hedgehog Is Required for the Proliferation and Specification of Ovarian Somatic Cells prior to Egg Chamber Formation in *Drosophila*.” *Development* 122 (4): 1125–35.
- Forbes, A. J., A. C. Spradling, P. W. Ingham, and H. Lin. 1996. “The Role of Segment Polarity Genes during Early Oogenesis in *Drosophila*.” *Development* 122 (10): 3283–94.
- Frantz, Christian, Anastasios Karydis, Perihan Nalbant, Klaus M. Hahn, and Diane L. Barber. 2007. “Positive Feedback between Cdc42 Activity and H⁺ Efflux by the Na-H Exchanger NHE1 for Polarity of Migrating Cells.” *The Journal of Cell Biology* 179 (3): 403–10.
- Ge, Lin, Wenxia Meng, Hongmei Zhou, and Neil Bhowmick. 2010. “Could Stroma Contribute to Field Cancerization?” *Medical Hypotheses* 75 (1): 26–31.
- Grillo-Hill, Bree K., Changhoon Choi, Maite Jimenez-Vidal, and Diane L. Barber. 2015. “Increased H⁺ Efflux Is Sufficient to Induce Dysplasia and Necessary for Viability with Oncogene Expression.” *eLife* 4 (March). doi:10.7554/eLife.03270.
- Grillo-Hill Bree K Choi Changoon; Jimenez-Vidal Maite Barber, Diane. 2015. “Increased H⁺ Efflux Is Sufficient to Induce Dysplasia and Necessary for Viability with Oncogene Expression.” *eLife* 03270 (March).
- Grillo-Hill, Bree K., Bradley A. Webb, and Diane L. Barber. 2014. “Ratiometric Imaging of pH Probes.” *Methods in Cell Biology* 123: 429–48.
- Hughes, Adam L., and Daniel E. Gottschling. 2012. “An Early Age Increase in Vacuolar pH Limits Mitochondrial Function and Lifespan in Yeast.” *Nature* 492 (7428). Nature Publishing Group: 261–65.

- Populations: Lessons from Embryonic Development.” *Cell* 132 (4): 661–80.
- Nystul, Todd G., and Allan Spradling. 2007. “An Epithelial Niche in the *Drosophila* Ovary Undergoes Long-Range Stem Cell Replacement.” *Cell Stem Cell* 1 (3). Elsevier Ltd: 277–85.
- . 2010. “Regulation of Epithelial Stem Cell Replacement and Follicle Formation in the *Drosophila* Ovary.” *Genetics* 184 (2). Genetics Soc America: 503–15.
- Owusu-Ansah, Edward, and Utpal Banerjee. 2009. “Reactive Oxygen Species Prime *Drosophila* Haematopoietic Progenitors for Differentiation.” *Nature* 461 (7263): 537–41.
- Pagliuca, Felicia W., and Douglas A. Melton. 2013. “How to Make a Functional β -Cell.” *Development* 140 (12): 2472–83.
- Parchem, Ronald J., Julia Ye, Robert L. Judson, Marie F. LaRussa, Raga Krishnakumar, Amy Blelloch, Michael C. Oldham, and Robert Blelloch. 2014. “Two miRNA Clusters Reveal Alternative Paths in Late-Stage Reprogramming.” *Cell Stem Cell* 14 (5). Elsevier Ltd: 617–31.
- Perkins, James R., John M. Dawes, Steve B. McMahon, David L. H. Bennett, Christine Orengo, and Matthias Kohl. 2012. “ReadqPCR and NormqPCR: R Packages for the Reading, Quality Checking and Normalisation of RT-qPCR Quantification Cycle (Cq) Data.” *BMC Genomics* 13 (July): 296.
- Pfeiffer, Jason, David Johnson, and Keith Nehrke. 2008. “Oscillatory Transepithelial H⁺ Flux Regulates a Rhythmic Behavior in *C. Elegans*.” *Current Biology: CB* 18 (4): 297–302.
- Pignoni, F. F., and S. L. S. L. Zipursky. 1997. “Induction of *Drosophila* Eye Development by Decapentaplegic.” *Development* 124 (2): 271–78.
- Price, Mary Ann, and Daniel Kalderon. 2002. “Proteolysis of the Hedgehog Signaling Effector Cubitus Interruptus Requires Phosphorylation by Glycogen Synthase Kinase 3 and Casein Kinase 1.” *Cell* 108 (6): 823–35.

- Larkin, M. K., K. Holder, C. Yost, E. Giniger, and H. Ruohola-Baker. 1996a. "Expression of Constitutively Active Notch Arrests Follicle Cells at a Precursor Stage during *Drosophila* Oogenesis and Disrupts the Anterior-Posterior Axis of the Oocyte." *Development* 122 (11): 3639–50.
- . 1996b. "Expression of Constitutively Active Notch Arrests Follicle Cells at a Precursor Stage during *Drosophila* Oogenesis and Disrupts the Anterior-Posterior Axis of the Oocyte." *Development* 122 (11): 3639–50.
- Li, Shuang, Yongbin Chen, Qing Shi, Tao Yue, Bing Wang, and Jin Jiang. 2012. "Hedgehog-Regulated Ubiquitination Controls Smoothed Trafficking and Cell Surface Expression in *Drosophila*." *PLoS Biology* 10 (1): e1001239.
- Li, Xiuju, Pratap Karki, Lei Lei, Huayan Wang, and Larry Fliegel. 2009. "Na⁺/H⁺ Exchanger Isoform 1 Facilitates Cardiomyocyte Embryonic Stem Cell Differentiation." *American Journal of Physiology. Heart and Circulatory Physiology* 296 (1): H159–70.
- Malo, Mackenzie E., Liang Li, and Larry Fliegel. 2007. "Mitogen-Activated Protein Kinase-Dependent Activation of the Na⁺/H⁺ Exchanger Is Mediated through Phosphorylation of Amino Acids Ser770 and Ser771." *The Journal of Biological Chemistry* 282 (9): 6292–99.
- Margolis, J., and A. Spradling. 1995. "Identification and Behavior of Epithelial Stem Cells in the *Drosophila* Ovary." *Development* 121 (11): 3797–3807.
- Miesenböck, G., D. A. De Angelis, and J. E. Rothman. 1998. "Visualizing Secretion and Synaptic Transmission with pH-Sensitive Green Fluorescent Proteins." *Nature* 394 (6689): 192–95.
- Murry, Charles E., and Gordon Keller. 2008a. "Differentiation of Embryonic Stem Cells to Clinically Relevant Populations: Lessons from Embryonic Development." *Cell* 132 (4): 661–80.
- . 2008b. "Differentiation of Embryonic Stem Cells to Clinically Relevant

- Hulikova, Alzbeta, Nicholas Aveyard, Adrian L. Harris, Richard D. Vaughan-Jones, and Pawel Swietach. 2014. "Intracellular Carbonic Anhydrase Activity Sensitizes Cancer Cell pH Signaling to Dynamic Changes in CO₂ Partial Pressure." *The Journal of Biological Chemistry* 289 (37): 25418–30.
- Jia, Jianhang, Lei Zhang, Qing Zhang, Chao Tong, Bing Wang, Fajian Hou, Kazuhito Amanai, and Jin Jiang. 2005. "Phosphorylation by Double-Time/CKI ϵ and CKI α Targets Cubitus Interruptus for Slimb/ β -TRCP-Mediated Proteolytic Processing." *Developmental Cell* 9 (6): 819–30.
- Khacho, Mireille, Alysén Clark, Devon S. Svoboda, Joelle Azzi, Jason G. MacLaurin, Cynthia Meghaizel, Hiromi Sesaki, et al. 2016. "Mitochondrial Dynamics Impacts Stem Cell Identity and Fate Decisions by Regulating a Nuclear Transcriptional Program." *Cell Stem Cell*, May. doi:10.1016/j.stem.2016.04.015.
- Kirilly, Daniel, Eric P. Spana, Norbert Perrimon, Richard W. Padgett, and Ting Xie. 2005. "BMP Signaling Is Required for Controlling Somatic Stem Cell Self-Renewal in the *Drosophila* Ovary." *Developmental Cell* 9 (5): 651–62.
- Koivusalo, Mirikka, Christopher Welch, Hisayoshi Hayashi, Cameron C. Scott, Moshe Kim, Todd Alexander, Nicolas Touret, Klaus M. Hahn, and Sergio Grinstein. 2010. "Amiloride Inhibits Macropinocytosis by Lowering Submembranous pH and Preventing Rac1 and Cdc42 Signaling." *The Journal of Cell Biology* 188 (4): 547–63.
- Kurosawa, Hiroshi. 2007. "Methods for Inducing Embryoid Body Formation: In Vitro Differentiation System of Embryonic Stem Cells." *Journal of Bioscience and Bioengineering* 103 (5): 389–98.
- Lancaster, Madeline A., Magdalena Renner, Carol-Anne Martin, Daniel Wenzel, Louise S. Bicknell, Matthew E. Hurles, Tessa Homfray, Josef M. Penninger, Andrew P. Jackson, and Juergen A. Knoblich. 2013. "Cerebral Organoids Model Human Brain Development and Microcephaly." *Nature* 501 (7467): 373–79.

- Robinton, Daisy A., and George Q. Daley. 2012. "The Promise of Induced Pluripotent Stem Cells in Research and Therapy." *Nature* 481 (7381): 295–305.
- Rossano, Adam J., Amit K. Chouhan, and Gregory T. Macleod. 2013. "Genetically Encoded pH-Indicators Reveal Activity-Dependent Cytosolic Acidification of *Drosophila* Motor Nerve Termini in Vivo." *The Journal of Physiology* 591 (7): 1691–1706.
- Sahai-Hernandez, Pankaj, and Todd G. Nystul. 2013. "A Dynamic Population of Stromal Cells Contributes to the Follicle Stem Cell Niche in the *Drosophila* Ovary." *Development* 140 (22): 4490–98.
- Schönichen, André, Bradley A. Webb, Matthew P. Jacobson, and Diane L. Barber. 2013. "Considering Protonation as a Posttranslational Modification Regulating Protein Structure and Function." *Annual Review of Biophysics* 42: 289–314.
- Shi, Qing, Shuang Li, Jianhang Jia, and Jin Jiang. 2011. "The Hedgehog-Induced Smoothed Conformational Switch Assembles a Signaling Complex That Activates Fused by Promoting Its Dimerization and Phosphorylation." *Development* 138 (19): 4219–31.
- Smelkinson, Margery G., Qianhe Zhou, and Daniel Kalderon. 2007. "Regulation of Ci-SCF^{Slimb} Binding, Ci Proteolysis, and Hedgehog Pathway Activity by Ci Phosphorylation." *Developmental Cell* 13 (4): 481–95.
- Song, X., and T. Xie. 2003. "Wingless Signaling Regulates the Maintenance of Ovarian Somatic Stem Cells in *Drosophila*." *Development* 130 (>14): 3259–68.
- Tesar, Paul J., Josh G. Chenoweth, Frances A. Brook, Timothy J. Davies, Edward P. Evans, David L. Mack, Richard L. Gardner, and Ronald D. G. McKay. 2007. "New Cell Lines from Mouse Epiblast Share Defining Features with Human Embryonic Stem Cells." *Nature* 448 (7150): 196–99.
- TwoRoger, M., M. K. Larkin, Z. Bryant, and H. Ruohola-Baker. 1999. "Mosaic Analysis in the *Drosophila* Ovary Reveals a Common Hedgehog-Inducible Precursor Stage for

- Stalk and Polar Cells.” *Genetics* 151 (2). Genetics Soc America: 739–48.
- Wagner, Jamie, Erik Allman, Ashley Taylor, Kiri Ulmschneider, Timothy Kovanda, Bryne Ulmschneider, Keith Nehrke, and Maureen a. Peters. 2011. “A Calcineurin Homologous Protein Is Required for Sodium-Proton Exchange Events in the *C. Elegans* Intestine.” *American Journal of Physiology. Cell Physiology* 301 (6): C1389–1403.
- Wang, Su, Yuan Gao, Xiaoqing Song, Xing Ma, Xiujuan Zhu, Ying Mao, Zhihao Yang, et al. 2015. “Wnt Signaling-Mediated Redox Regulation Maintains the Germ Line Stem Cell Differentiation Niche.” *eLife* 4 (October): e08174.
- Wray, Jason, Tuzer Kalkan, and Austin G. Smith. 2010. “The Ground State of Pluripotency.” *Biochemical Society Transactions* 38 (4): 1027–32.
- Ying, Qi Long, Jennifer Nichols, Ian Chambers, and Austin Smith. 2003. “BMP Induction of Id Proteins Suppresses Differentiation and Sustains Embryonic Stem Cell Self-Renewal in Collaboration with STAT3.” *Cell* 115 (3): 281–92.
- Ying, Qi-Long, Jason Wray, Jennifer Nichols, Laura Battle-Morera, Bradley Doble, James Woodgett, Philip Cohen, and Austin Smith. 2008. “The Ground State of Embryonic Stem Cell Self-Renewal.” *Nature* 453 (7194). Nature Publishing Group: 519–23.
- Young, Richard A. 2011. “Control of the Embryonic Stem Cell State.” *Cell* 144 (6): 940–54.
- Zhang, Chi, Elizabeth H. Williams, Yurong Guo, Lawrence Lum, and Philip A. Beachy. 2004. “Extensive Phosphorylation of Smoothened in Hedgehog Pathway Activation.” *Proceedings of the National Academy of Sciences of the United States of America* 101 (52): 17900–907.
- Zhang, Yan, and Daniel Kalderon. 2001. “Hedgehog Acts as a Somatic Stem Cell Factor in the *Drosophila* Ovary” 6: 599–604.
- Zhang, Y., and D. Kalderon. 2000. “Regulation of Cell Proliferation and Patterning in

Drosophila Oogenesis by Hedgehog Signaling.” *Development* 127 (10): 2165–76.
Zhao, Yun, Chao Tong, and Jin Jiang. 2007. “Hedgehog Regulates Smoothed Activity by Inducing a Conformational Switch.” *Nature* 450 (7167): 252–58.

Appendices

Code Appendix

I used RStudio to perform statistics and generate plots of the majority of the experiments described in this body of work. The code used to generate plots is published on Rpubs, and links to code plots and code are described below.

The code for generating [three-point and two-point calibrations](#) for initial pHlourin experiments. The plots in Figure 3C-D and Table 1 are derived from this code.

An example of how to calculate pH values from ratio values and the code for the plot of Figure 4C can be found [here](#). To calculate pH values from ratios I first separated the wildtype and mutant calibration data. Then, I generated linear regression models for wildtype and mutant. Then, I calculated pH values separately using separate linear regression models for each cell type. I then combined the wildtype and mutant data back into a single data frame, and repeated this calculation using the same code for each separate .csv file for each experiment. To make the final plot, I removed values outside the linear range of the data, and then made the plot.

The code for generating the plot of the [egg laying assay](#). This plot is in Figure 5A.

The code for generating the plot of the [Nhe2 morphological phenotypes](#). This plot is in Figure 5B.

The code for generating [ptc RNAi data and smoGFP data](#). The plots in Figures 6D, 7G, 10D, 10G, and 11 E-F are derived from this code.

Publishing Agreement

It is the policy of the University to encourage the distribution of all theses, dissertations, and manuscripts. Copies of all UCSF theses, dissertations, and manuscripts will be routed to the library via the Graduate Division. The library will make all theses, dissertations, and manuscripts accessible to the public and will preserve these to the best of their abilities, in perpetuity.

Please sign the following statement:

I hereby grant permission to the Graduate Division of the University of California, San Francisco to release copies of my thesis, dissertation, or manuscript to the Campus Library to provide access and preservation, in whole or in part, in perpetuity.

Bryne Umsehreids
Author Signature

8/17/16
Date